(Received 14 January 2026, Accepted 25 February 2026, Scheduled 13 April 2026)

Microwave Wire Media: Theory and Main Physical Effects

Denis I. Sakhno[1], Constantin R. Simovski[2], and Pavel A. Belov[1, 3, *]

[1] School of Physics and Engineering, ITMO University, Kronverksky Pr. 49, St. Petersburg 197101, Russia
[2] Department of Electronics and Nanoengineering, Aalto University, P.O. Box 15500, Espoo, Finland
[3] School of Engineering, New Uzbekistan University, Movarounnahr str. 1, Tashkent 100000, Uzbekistan

ABSTRACT: We present a review of homogenization models of microwave wire media with different geometries. We begin with a simple (uniaxial) wire medium and then consider more complex types of wire media — double, triple, and interlaced wire media — which remain underexplored. We discuss boundary problems with wire media and the most important physical effects revealed using the reviewed homogenization models.

1. INTRODUCTION

Wire media (WM) are electromagnetically dense arrays of thin metal wires. Most of wire media are regular lattices, which were earlier reviewed in [1]; however, there are also tapered WM operating in microwave, THz, and visible ranges [2–6]. There are also irregular wire media, sometimes called metal brushes [7–10]. For regular WM, the electromagnetic density means that the lattice period a is small compared to the wavelength λ in free space. For irregular WM, the concept is similar, with a being the mean distance between two adjacent wires. The electromagnetic density of the array allows homogenizing WM, i.e., describing their electromagnetic properties in terms of macroscopic (mean) fields and material parameters. Within the framework of the homogenization model, WM are effectively continuous and, therefore, can be called materials. At higher frequencies, where a approaches λ and exceeds it, regular lattices of wires are called metallic photonic crystals.

Artificial effectively continuous media (composite materials) with unusual and useful properties not observable in natural materials are called metamaterials. This definition can be found in [11–16] and in numerous reviews on metamaterials. Nowadays, the terminology is commonly adopted. All known types of WM are metamaterials, and below we will explain why.

Wire metamaterials have found numerous applications in the ultrabroad spectrum from radio-frequencies (see, e.g., [17, 18]) to the near-infrared and visible light ranges (see, e.g., [19–24]). Different types of WM manifest different electromagnetic behavior, and even the same type of WM can possess different properties in different frequency ranges. At radio frequencies and microwaves, low-loss metals, such as copper, silver, aluminum, and brass, are good conductors, which enable the approximation of perfect electrical conductors (PEC). In the visible range, low-loss metals such as gold and silver are plasmonic, which makes the wires (nanowires) of optical WM self-resonant. The area of WM is too broad to be covered in a single review. Here, we concentrate on the analytical modeling of microwave WM and briefly discuss their main physical effects without going into corresponding applications.

Most metamaterials exhibit unusual properties due to resonances of their structural elements. This is not the case for microwave WM: their unique properties originate from their inherent strong spatial dispersion. This dispersion is manifested in the resonant dependence of the effective permittivity of WM on the wave vector. Sometimes, this property is explained by the infinite length of the wires adopted by the homogenization model (see Chapter 3 of [15]) as follows. If the structural element of a lattice (in this case, a wire) is not small compared to λ, a conventional quasi-static homogenization (see, e.g., in [25]) cannot be applied. It is replaced by a formal homogenization similar to that applied to photonic crystals. This formal homogenization relates the Bloch harmonics of the medium polarization to the Bloch harmonics of a wave with a given wave vector $\mathbf{q}$. Consequently, the effective permittivity of a photonic crystal depends on $\mathbf{q}$. However, the applicability of this permittivity for solving boundary problems is questionable. In [26], a honeycomb photonic crystal with a dielectric host and air holes shows different material parameters for different locations of interfaces. Such material parameters are called mesoscopic.

Another example of mesoscopic material parameters is a pair of effective permittivity and effective permeability of a periodic bilayer structure with electromagnetically thin bilayers of two different dielectrics (see, e.g., in [27]). These parameters are retrieved from the reflection and transmission coefficients of the structure excited by a plane wave with a given angle of incidence and polarization. However, this pair of parameters has no physical meaning, because it comprises a non-trivial effective permittivity even for structures without magnetic polarization. In fact, mesoscopic material parameters are useless, since they provide a simple analytical solution to only one boundary problem — the very problem whose numerical solution was used to retrieve these parameters (see in Chapter 11 of [14]). They are not suitable for different boundary problems (even with the same interfaces, but different excitation).

* Corresponding author: Pavel A. Belov (belov@metalab.ifmo.ru).

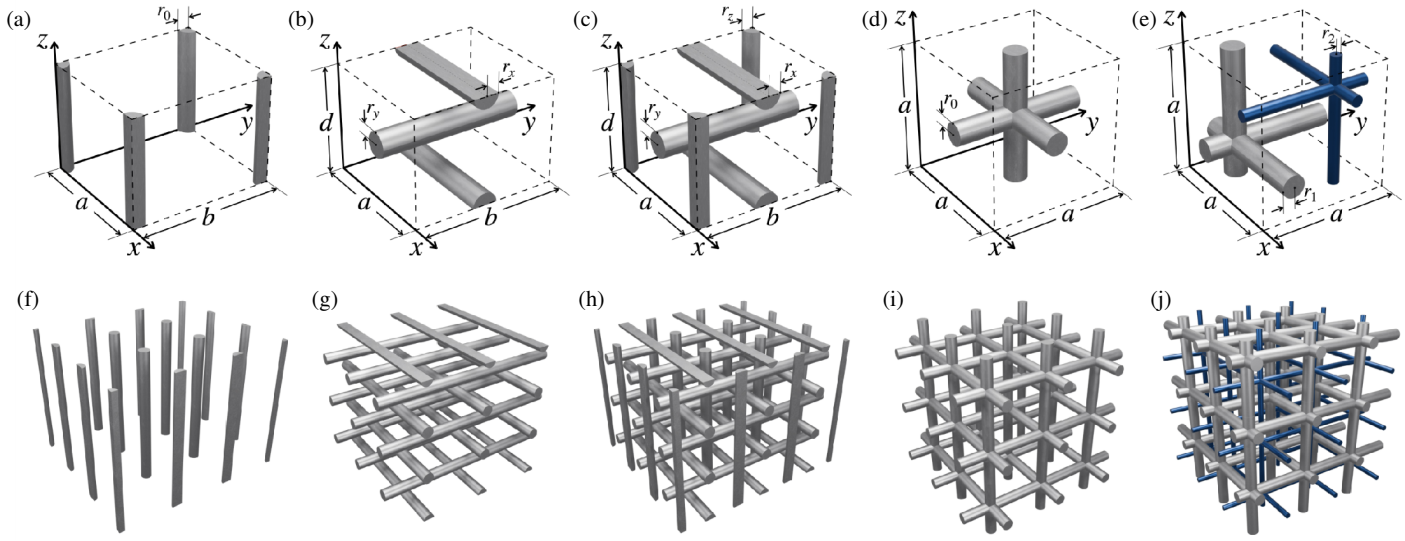

FIGURE 1. Unit cells of different WM and their general views, respectively. (a), (b) Simple WM. (c), (d) Double WM. (e), (f) Triple non-connected wire medium. (g), (h) Triple connected WM. (i), (j) Double interlaced WM.

Homogenization models of WM are not formal, because the effective permittivity calculated for an infinite unbounded WM is not mesoscopic. It properly describes the properties of finite samples, such as WM endoscopes and layers. Moreover, models developed for infinite wires work for electromagnetically short wires. A well-known example is the so-called *mushroom metasurfaces*, in which the wire length may be of the order of $\lambda/100$. Mushroom metasurfaces, also called high-impedance surfaces and artificial magnetic walls, are electromagnetically dense arrays of coplanar metal patches located at a distance $h \ll \lambda$ from a metal plane [28]. Each patch was connected to a metal plane with a metal pin of length h. Ref. [29] assumed that an array of these short wires can be treated as a very thin layer of WM sandwiched between the metal ground plane and metal patches. This assumption was confirmed by further studies ([30–33], etc.), showing that the spatially dispersive permittivity of WM offers a highly accurate description of the electromagnetic properties of mushroom metasurfaces.

The spatial dispersion of WM effective permittivity results from the electromagnetic interaction between the wires. This interaction may be strong even for very short wires, if they have specific terminations. We will discuss this further, in the context of the so-called additional boundary conditions. Spatial dispersion is an essential physical phenomenon in WM, and we pay special attention to it in this review. Most physical effects in WM discussed in this review arise due to spatial dispersion. The only exception is epsilon-near-zero materials; however, they should also be considered in the context of spatially dispersive permittivity. We also discuss the impact of finite losses in the wires, energy density and power flux in WM, WM boundary problems, and key physical effects observed in WM.

Practically important regular microwave WM can be classified into the following groups:

- Simple WM: an array of wires oriented along a particular direction. This type of WM can comprise unloaded or periodically loaded wires and can also be nested (formed by wires of different radii);
- Double WM: an array of wires oriented along two different (usually orthogonal) directions. Wires directed along different directions may either touch or not; thus, the double WM can be connected or disconnected;
- Triple WM: an array of wires oriented along three different (usually orthogonal) directions. Similarly to double WM, wires directed along different directions may either touch or not, and the triple WM can be connected or disconnected;
- Interlaced WM: a structure formed by triple connected WM embedded one into another without connection.

These types of WM are illustrated by Fig. 1. We start our review from a simple WM, which has quite a long history and numerous applications, and it is better investigated than other types of WM.

A few comments about notations. We did our best to maintain uniform notations throughout the paper. For this purpose, we changed the original notations where necessary. In these cases, we indicate that the notations have been changed. The WM plasma frequency is denoted as ω_p, the plasma wavenumber $k_p = \omega_p/c = 2\pi/\lambda_p$, where c is the vacuum speed of light, and λ_p is the plasma wavelength. The wavenumber of free space is denoted as $k = \omega/c$, and the wave vector inside a WM $\mathbf{q}$. If a WM consists of wires with the same radius, it is denoted as r_0. The imaginary unit is j.

2. SIMPLE WIRE MEDIA

2.1. Brief History

The pioneering work by Von Ignatowsky [34] on a regular planar array of thin, parallel, perfectly conducting wires illuminated by a plane wave was continued by the analysis of the

transmissive and reflective properties of this array in [35]. In this paper, a planar grid of thin PEC wires was considered as a flat semitransparent surface; a wave with electric field parallel to the wires was shown to be fully reflected at low frequencies and almost fully transmitted at high frequencies (see also [36, 37], where wires with a finite impedance per unit length were considered). These early studies were the prehistory of WM.

The history of WM started from a microwave lens of wires suggested and experimentally studied by Kock in [38, 39]. A dipole-type antenna operating at 6 GHz created radiation with transverse magnetic polarization, with the magnetic field vector and the wave vector lying in the xy plane, and the electric field directed along the z axis (see Fig. 1(a)). To shape the radiated beam, a material was needed with the axial component ε_{zz} of the permittivity tensor spatially varying in the xy plane. The manufacturing technologies of dielectric composites existing at that time could not achieve the required permittivity gradient. Therefore, Kock suggested an artificial uniaxial dielectric formed by thin metal wires oriented along z with a spatially varying interwire distance. This hypothesis used the knowledge that in a planar grid of wires oriented along z, quite noticeable currents can be induced by z-polarized electric field, even at high frequencies, where the grid is transparent [35]. Kock assumed that these currents induced in an electromagnetically dense set of such grids should result in a delay of the transmitted wave, and an entire array of wires should act as a dielectric. Refs. [38, 39] experimentally confirmed this hypothesis, and the spatially varying effective refractive index of the artificial dielectric was retrieved.

The first analytical model of an unbounded array of thin parallel wires rigorously explaining the operation of the Kock lens was developed by Brown in [40] for in-plane (xy) propagation of waves with transverse magnetic (TM) polarization with respect to the wires. In that work, the effective axial permittivity ε_{zz} of the lattice was introduced for frequencies higher than the plasma frequency. In further works by Brown and Rotman [41, 42], the effective-medium model was extended to lower frequencies. The dispersion equation was derived for waves propagating across a simple WM, and the low-frequency cutoff ω_p was found for TM-polarized waves. Both these works showed that below this frequency, the axial component of the permittivity tensor becomes negative, and its dispersion is similar to that of a natural plasma. At frequencies slightly higher than ω_p, natural plasmas are super-refractive: $\mathrm{Re}(\varepsilon_{\mathrm{plasma}}) < 1$, and the same holds for ε_{zz} for an electromagnetically dense lattice of wires parallel to the z axis. Thus, since early 1960s, it has been known that an electromagnetically dense lattice of parallel wires not only is an artificial dielectric for TM-polarized waves propagating across the wires, but also becomes effective microwave plasma near the characteristic frequency ω_p.

These lattices deserved a specific terminology. In [43] (by the group of Brown), they were called *rodded media*. An alternative term *thin-wire structures* was suggested in [44, 45] by Pendry et al. (these papers repeated the main results obtained by Brown and Rotman). Finally, in works by Belov et al. [46–48], the term *wire medium* was introduced. The terms *simple, double, and triple WM* appeared in 2004–2006 in [49–51]. Since that time, this terminology has been commonly adopted (see, e.g., in [1]).

Two main types of simple wire media are lattices with (1) a rectangular unit cell [46, 48, 52–54] and (2) a triangular one [55–57]. Their electromagnetic properties differ above the plasma frequency. In this range, TM waves can propagate in a WM, and two corresponding dispersion curves intersect for a triangular lattice [57] and converge at a point X of the Brillouin zone for a square lattice. Below the plasma frequency, only the waves with electric field orthogonal to the wires may propagate in a lossless simple WM (see Subsection 2.2). At these frequencies, there is no qualitative difference between the electromagnetic properties of triangular and square WM.

In this paper, we do not review triangular wire lattices, concentrating on a more popular simple WM with rectangular unit cells, as in Figs. 1(a)–(b). This WM is a double-periodic $a \times b$ array of infinite wires oriented along the z axis. The array is located in an isotropic dielectric host, e.g., free space. By definition, the term WM implies that its periods are electromagnetically small, i.e., $a < \lambda/2$ and $b < \lambda/2$. As discussed above, at higher frequencies, a WM is not a material, but a photonic crystal. Further, we will show that the condition of electromagnetically small periods allows operation frequencies significantly higher than ω_p. The condition of thin wires ($r_0 \ll a$ and $r_0 \ll b$) is also conceptually important for WM.

Simple WM of parallel copper strips of strongly subwavelength width $w \ll \lambda$ fabricated on dielectric sheets were studied at frequencies notably higher than ω_p in [58, 59]. Since at these frequencies, $\varepsilon_{zz} > 1$, the main effect was refraction, and these simple WM were called *strip-type artificial dielectrics*. We mention these works, because they have shown that the wire cross-section shape barely matters for a simple WM if $w \ll a$. A metal strip is equivalent to a circular metal wire with radius $r_0 = w/4$.

In 1960–1970s, the dielectric composite technologies became more advanced, and the practical need in WM ceased, which demotivated the researchers from exploration of this area. The topic of simple WM revived in the late XX and early XXI centuries due to the development of metamaterials by Pendry. In [44], Pendry et al. showed that a lattice of parallel thin wires has a negative effective permittivity at frequencies below its effective plasma frequency ω_p for waves propagating in the xy-plane with a z-polarized electric field. Therefore, this lattice can serve as a negative-epsilon host for a composite with a negative permeability. As the negative-mu composite, an electromagnetically dense lattice of resonant magnetic scatterers (called *split-ring resonators*) was chosen. Split-ring resonators (SRRs) suggested by Pendry were concentric double rings of copper strips with narrow splits playing the role of capacitive loads. SRRs provided negative permeability at frequencies slightly higher than their Lorentzian resonance frequency. In this narrow frequency band, a combined lattice of both parallel wires and SRRs was predicted to be a material with a negative refractive index (for TM-polarized waves propagating in the xy-plane).

The concept of negative-index media, also called *left-handed media*, was introduced in 1968 by Veselago in [60]. Veselago showed that a hypothetic medium with both negative permittivity and permeability has negative (anti-Snell's) refraction, which may be useful for some applications. As an example, a layer of medium with relative permittivity and permeability both equal to -1 was predicted to act as an aberration-free pseudo-lens [60]. In 2000, in [61], Pendry hypothesized that the Veselago pseudo-lens should be a perfect lens — i.e., create a point image of a point source in the far zone of the source. This work attracted a lot of attention to Veselago's left-handed media.

Next, researchers needed to prove that these metamaterials are feasible. Their uniaxial version based on WM and SRRs was simulated and built by the group of Smith [62]. SRRs lying in the xz and yz planes formed a cubic lattice and were centered exactly in the middle between two adjacent wires of a simple WM. Negative real part of the complex refractive index and smallness of its imaginary part were shown theoretically in [62] and experimentally in [63]. Isotropic (with a negative scalar refractive index) left-handed metamaterials have been designed and experimentally studied in several works since 2004, when Refs. [64, 65] were published. Works in this area are not discussed in the present paper, because WM were not utilized in them.

Electromagnetic waves whose wave vector forms an arbitrary angle with the wires of a simple WM were studied in 2003 in pioneering work [48]. Later, the homogenization model of WM was numerically and experimentally validated in many works. This model is reviewed in the next subsection.

2.2. Nonlocal Permittivity of Simple Wire Media of Perfect Electrical Conductors

An effective medium model of a simple WM was suggested in [48] based on the approximation of PEC wires ($|\varepsilon_{\text{metal}}| \to \infty$) and $r_0 \ll a,\, b \ll \lambda$. The PEC approximation is adequate for microwave WM formed by any metal if the condition of minimal possible wire radius r_0 is satisfied [66]. Namely, the wire radius must be at least an order of magnitude larger than the skin depth of the metal forming the wires. For copper (Cu) at 1–10 GHz, this condition yields $r_0 > 20$ μm, because the copper skin depth in this band is within (0.7–2) μm. Therefore, for copper wires, $r_0 = [0.02, 3]$ mm satisfies both the minimal possible wire radius condition (which allows the PEC approximation) and the condition of thin wires (which means that the lattice is a simple WM). The theory of WM with finite losses, which allows checking whether the PEC approximation is suitable for a certain wire radius, will be explored in Subsection 2.3. We will also discuss particular problems in which losses must be accounted for even for wires with a suitable radius.

For a simple WM of PEC wires in a dielectric host of isotropic permittivity $\varepsilon_{\text{host}}$, as well as for any uniaxial material, the permittivity tensor has the following form:

$$\bar{\bar{\varepsilon}}_{\text{simple}} = \varepsilon_{\text{host}} \left(\hat{\mathbf{u}}_x \hat{\mathbf{u}}_x + \hat{\mathbf{u}}_y \hat{\mathbf{u}}_y\right) + \varepsilon_{zz} \hat{\mathbf{u}}_z \hat{\mathbf{u}}_z. \tag{1}$$

Here, $\hat{\mathbf{u}}_\alpha$ are unit vectors, and $\hat{\mathbf{u}}_\alpha \hat{\mathbf{u}}_\alpha$ are unit dyads, where $\alpha = (x, y, z)$.

In [48], the axial permittivity covering all possible eigenmodes of a simple WM was derived:

$$\varepsilon_{zz}(\omega, q_z) = \varepsilon_{\text{host}} \left(1 - \frac{k_p^2}{\varepsilon_{\text{host}} \left(\frac{\omega}{c}\right)^2 - q_z^2}\right), \tag{2}$$

where $k_p \equiv \omega_p / c$ is the plasma wave number. This result was obtained using the local field approach, earlier applied to eigenwaves propagating in-plane in [46]. In the model of [48], an eigenwave with the wave vector $\mathbf{q} = (q_x, q_y, q_z)^T$ and electric field amplitude $\mathbf{E}$ propagates obliquely to the axis z, being supported by the line currents $I_{m,n}(z)$ flowing along z. The vector $\mathbf{q}$ determines the phase shifts between the wires, and the local field acting on a reference wire $(m = n = 0)$ is created by currents of all other wires. Since the complex amplitudes of all currents differ only by the phases, this local field is proportional to $I_{0,0}$. The current response of a PEC wire of finite radius r_0 to this local field can be expressed in terms of cylindrical functions, as well as the local field. This approach allows relating the currents $I_{0,0}$ with the amplitude $\mathbf{E}$ referred to the axis of the reference wire. Currents in the wires form the mean (macroscopic) current density $\mathbf{J}(x, y, z)$, obtained by extending the line currents over the unit cell cross section of area ab. The mean medium polarization $\mathbf{P} = P\hat{\mathbf{z}}$ is related with $\mathbf{J}$ by continuity equation, which in the present one-component case takes the form $J = j\omega P$. Thus, the axial component of the electric displacement $D_z \equiv \varepsilon_0 E_z + P$ can be expressed via the axial component E_z of the eigenwave amplitude to find the axial permittivity defined by the standard relation $D_z = \varepsilon_0 \varepsilon_{zz} E_z$.

To obtain the axial permittivity in a simple closed form (2), the series of cylindrical functions were converted into exponentially convergent ones, which allowed truncating the infinite series. Some asymptotics of cylindrical functions were also used. In this, the model followed the previous work [46]. In [46], the following formula was derived for the plasma wave number (valid for the case $r_0/a < 0.1$ and $\varepsilon_{\text{host}} = 1$):

$$k_p^2(a, b, r_0) = \left(\frac{\omega_p}{c}\right)^2 = \frac{2\pi/ab}{\ln \frac{\sqrt{ab}}{2\pi r_0} + F(a/b)}, \tag{3}$$

where

$$F(a/b) = -\frac{1}{2} \ln \frac{a}{b} + \sum_{n=1}^{\infty} \frac{\coth\left(\pi n \frac{a}{b}\right) - 1}{n} + \frac{\pi}{6} \frac{a}{b}. \tag{4}$$

This formula proved to be more accurate than the previously derived plasma frequency from [45] and earlier works. Later studies [53, 69–71] produced multiple approximate formulas for k_p corresponding to different values of the ratios r_0/a, r_0/b, restricted only by the evident requirement $r_0/a,\, r_0/b < 0.5$. These formulas are presented in Table 1 and discussed in detail in [70–72].

Figure 2 presents the numerically simulated dispersion diagram of a square lattice of thin PEC wires in free space in a broad frequency range, covering the range of normalized frequencies $ka > 2\pi$ (that of a metal photonic crystal, see above). To explain the bottom part of the dispersion diagram, which

TABLE 1. Analytical formulae for the plasma wavenumber k_p of a wire medium, including references to the works in which they were derived. Formulae correspond to a wire medium with a square lattice ($a = b$).

Authors	Ref.	Formulae for k_p^2
J.B. Pendry et al.	[44, 45]	$k_p^2 = \dfrac{2\pi/a^2}{\ln \frac{a}{r_0}}$
A.K. Sarychev et al.	[67]	$k_p^2 = \dfrac{2\pi/a^2}{\ln \frac{a}{\sqrt{2}r_0} + \frac{\pi}{4} - \frac{3}{2}}$
P.A. Belov et al.	[46, 48]	$k_p^2 = \dfrac{2\pi/a^2}{\ln \frac{a}{2\pi r_0} + \frac{\pi}{6} + \sum\limits_{n=1}^{\infty} \frac{\coth(\pi n)-1}{n}} \approx \dfrac{2\pi/a^2}{\ln \frac{a}{2\pi r_0} + 0.527}$
G.B. Shvets et al.	[68]	$k_p^2 = \dfrac{8/a^2}{\ln \frac{a}{2\sqrt{2}r_0}}$
A.V. Tyukhtin et al.	[53]	$k_p^2 = \dfrac{2\pi/a^2}{\ln \frac{a}{r_0} - 1.0487}$
S.I. Maslovski et al.	[52, 69]	$k_p^2 = \dfrac{2\pi/a^2}{\ln \frac{a^2}{4r_0(a-r_0)}}$
A. Kumar et al.	[70]	$k_p^2 = \dfrac{2\pi}{a^2}\left\{1.763\dfrac{r_0}{2a} + \left[1.264 + \ln\dfrac{a^2}{4r_0\left(\sqrt{2}a - r_0\right)}\right] - \frac{\sqrt{a^2-r_0^2}}{a}\left[\arctan\frac{r_0}{\sqrt{2}\sqrt{a^2-r_0^2}} + \arctan\frac{a}{\sqrt{a^2-r_0^2}}\right]\right\}^{-1}$

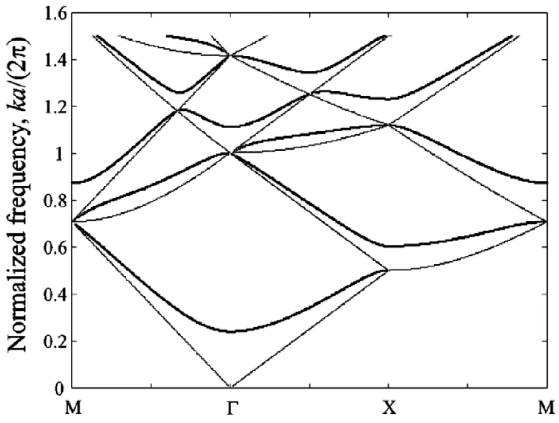

FIGURE 2. Dispersion diagram of a simple wire medium with a square unit cell ($a = b$, see Fig. 1). Filling ratio $\pi r_0^2/a^2$ is equal to 10^{-3}. Coordinates of the high symmetry points in the reciprocal space are $\Gamma = (0, 0, 0)^{\mathrm{T}}$, $\mathrm{X} = (\pi/a, 0, 0)^{\mathrm{T}}$, $\mathrm{M} = (\pi/a, \pi/a, 0)^{\mathrm{T}}$. Reproduced from [49] with the permission of publishers.

corresponds to a simple WM, we need to derive the dispersion equation. It follows from the general dispersion equation of an arbitrary anisotropic medium characterized by a dyadic permittivity (see, e.g., [25]):

$$\det\left(\mathbf{qq} - q^2\,\bar{\bar{\mathbf{I}}} + k^2\,\bar{\bar{\varepsilon}}\right) = 0, \tag{5}$$

where $\bar{\bar{\mathbf{I}}} = \sum_\alpha \hat{\mathbf{u}}_\alpha \hat{\mathbf{u}}_\alpha$ is the identity dyadic; $\mathbf{qq}$ is the dyadic of the wave vector; and $k = \omega/c$ is the free space wave number.

Substituting Eqs. (1) and (2) into Eq. (5) and dividing by $k_{\text{host}}^2 \equiv k^2\varepsilon_{\text{host}}$ (the wave number in the host medium) yields

$$\left(k_{\text{host}}^2 - q^2\right)\left(k_{\text{host}}^2 - k_p^2 - q^2\right)\left(k_{\text{host}}^2 - q_z^2\right) = 0, \tag{6}$$

where $k_p = k_p(a, b, r_0)$ can be found from (3). This relation defines three main modes of a simple WM.

2.2.1. TE-Modes

The modes propagating obliquely to the wires or perpendicular/parallel to them, with an electric field orthogonal to the wires, do not interact with wires. They are called *ordinary modes*, and their dispersion is described by the equation corresponding to the first bracket of relation (6):

$$q^2 = q_x^2 + q_y^2 + q_z^2 = k_{\text{host}}^2. \tag{7}$$

These modes are shown by thin lines in Fig. 2.

2.2.2. TM-Modes

The *extraordinary modes* are TM-polarized (their magnetic field is orthogonal to z), and their dispersion equation corresponds to the second bracket of relation (6):

$$q^2 = k_{\text{host}}^2 - k_p^2. \tag{8}$$

These modes are shown by thick lines in Fig. 2. They may propagate obliquely to z axis or perpendicular/parallel to it at frequencies above the plasma frequency. At lower frequencies, such TM-modes decay in one or more directions, since q is imaginary. For clarity, in this review, we will call the prop-

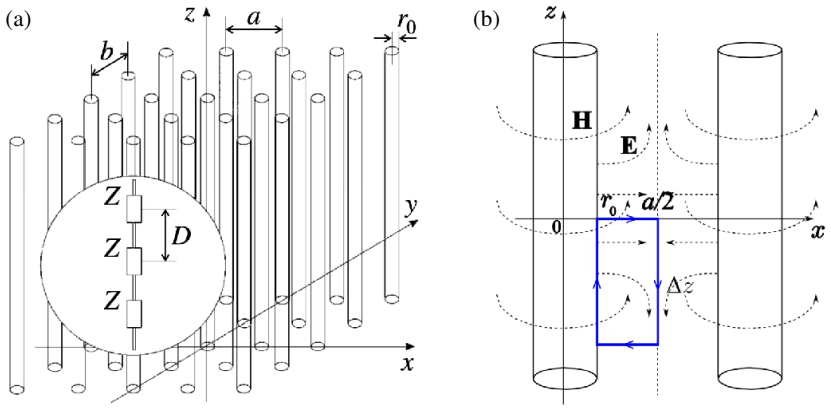

FIGURE 3. Wire medium composed of periodically loaded or lossy wires. Images are taken from: (a) [47], (b) [69], both with the permission of publishers. In (b), the integration contour l of the microscopic field **E** is shown.

agating modes *eigenwaves* and the attenuating modes *polaritons*. Let us explain the last term. In the theory of lossless photonic crystals, attenuating modes are called decaying or (more often) localized modes. Polaritons are a special case of localized modes — they are eigenmodes that propagate along an axis or in a plane and attenuate with distance away from this axis or from this plane (see, e.g., [73]). From (8), it follows that $q_x^2 + q_y^2 + q_z^2 = -\xi^2$, where $\xi^2 \equiv k_p^2 - k_{\text{host}}^2 > 0$. If q_z is real, the transverse wave number $\sqrt{q_x^2 + q_y^2}$ is imaginary, i.e., the eigenmode amplitude decays with distance away from the z axis. This polariton may be excited by an internal source located on the z axis. Its field weakly interacts with distant wires, screened by wires nearest to the z axis. If q_z is imaginary, the eigenmode field is localized in the xy plane, and the mode propagates in this plane, because $\sqrt{q_x^2 + q_y^2}$ is real. Such a polariton can be excited by a plane wave incident on the interface of a semi-infinite WM or by a source located near this interface.

In the case $-q_z^2 - \xi^2 > k^2$, we have $\sqrt{q_x^2 + q_y^2} > k$. This polariton may be a proper surface wave that propagates along the WM interface xy and decays away from it in both WM and free space. Below, we will discuss the role of polaritons arising in important boundary problems with simple WM.

2.2.3. TEM-Modes

The mode corresponding to the last brackets in Eq. (6) is described by the dispersion equation

$$q_z^2 = k_{\text{host}}^2. \tag{9}$$

At low frequencies $\omega < \omega_p$, probably, the most interesting mode of a simple WM is observed: a transverse electromagnetic (TEM) wave that can propagate only along the wires. This mode has planar isofrequency surfaces, since q_z does not depend on q_x and q_y. In other words, transverse wave numbers may be arbitrary, whereas q_z is equal to $\pm k_{\text{host}}$. For this eigenwave, our simple WM represents a multi-wire transmission line. The mean current density J supporting this mode equals to zero only in the trivial case $q_x = q_y = 0$, when the mode degenerates into a uniform plane wave. In this case, the TEM wave is ordinary, and it does not induce currents in the wires. If $q_x \neq 0$ or $q_y \neq 0$, the TEM mode is extraordinary.

The most important result of formula (2) is the insight into strong spatial dispersion achieved via the analysis of this low-frequency mode. The resonant singularity of the axial permittivity at $q_z = k_{\text{host}}$, which allows arbitrary q_x and q_y, has a clear physical meaning. If $q_x \neq 0$ or $q_y \neq 0$, the WM is an unbounded transmission line, whose field is not uniform in the transverse (xy) plane. As discussed above, the mean current density supporting such an eigenwave is nonzero. Therefore, $P_z \neq 0$ and $D_z \neq 0$ despite $E_z = 0$, which means that the permittivity $\varepsilon_{zz} = D_z/E_z\varepsilon_0$ must be infinite.

Note that the phase non-uniformity of the mode field in the plane xy does not imply phase transfer along x or y. The phase velocity of this mode is well directed along z, as well as the group velocity and the power flux. This regime cannot hold in plasmas, even magnetized and spatially dispersive ones (see, e.g., in [74]). It is the most unusual property of a simple microwave WM, which allows categorizing it as a metamaterial.

Additionally, [48] has shown that the effective axial permittivity (2) satisfies the causality principle and gives physical solutions for a hollow metal waveguide filled with WM. These studies gave the first arguments confirming that the spatially dispersive homogenization model should be valid for realistic finite-size WM samples.

2.3. Simple Wire Medium of Realistic Wires

Ref. [47] suggested engineering the frequency dispersion properties of a simple WM using periodically loaded wires instead of simple metal ones. Identical lumped impedances $Z(\omega)$ can be inserted along each wire with period D, as shown in Fig. 3(a). In this case, the plasma frequency expression (3) becomes

$$k_p^2(a, b, r_0, \mathcal{Z}) = \frac{2\pi/ab}{\ln\frac{\sqrt{ab}}{2\pi r_0} + F(a/b) - \frac{2\pi j}{\eta k}\mathcal{Z}(\omega)}, \tag{10}$$

where $\eta = \sqrt{\mu_0/\varepsilon_0}$ is the free-space impedance, and $\mathcal{Z}(\omega) = Z(\omega)/D$ is the wire impedance per unit length. The effective

permittivity tensor and dispersion are modified accordingly. Inductive loads red-shift the plasma frequency, which can be interpreted as an effective reduction of the wire radius (then, a radius smaller than the skin depth can be realized while keeping the PEC approximation suitable for realistic wires). Capacitive loads, in contrast, provide a low-frequency pass-band for TM-polarized waves propagating obliquely and perpendicular to the z axis. Note that the spatial dispersion in a C-loaded simple WM is preserved if $C_{\text{load}} \neq 0$. However, in this case, the spatial dispersion is not as strong as that in the unloaded WM. Even in the lossless approximation, ε_{zz} is no longer singular for real q_z if $\mathcal{Z}(\omega) = 1/j\omega DC_{\text{load}}$ is nonzero.

The concept of the impedance per unit length $\mathcal{Z}(\omega)$ was later used in the theory of simple WM of realistic wires — i.e., with finite conductivity. This theory was developed in [69]. The impedance per unit length of a wire with complex permittivity $\varepsilon_w = \varepsilon'_w - j\varepsilon''_w$, where $\varepsilon''_w = \sigma_w/\varepsilon_0\omega$ and σ_w is the conductivity of the wire material, is as follows: $Z_w = [j\omega\pi r_0^2\varepsilon_0(\varepsilon_w - 1)]^{-1}$. The individual impedance Z_w is in some sense equivalent to $\mathcal{Z}(\omega)$, but implies the impact of the finite conductivity and not of the load. If $|\varepsilon_m|$ is finite, the wires are lossy, and the local field approach of [48] is not applicable. Indeed, due to losses in the wires, the eigenwave of our WM attenuates in space. Therefore, the current $I_{m,n}$ in the (m,n)-numbered wire differs from the current $I_{0,0}$ in the reference wire in both phase and amplitude. Since the wave vector $\mathbf{q}$ is complex, the amplitudes of all currents also vary along z. Since the eigenmode problem cannot be analytically solved using the local field approach, in the pioneering work [69], the effective axial permittivity was obtained from specially derived telegrapher's equations of a lattice of lossy wires.

Work [69] starts from a true (microscopic) field $\mathbf{E}$ and the true current I_z flowing in the reference wire — the left one in Fig. 3(b). The electric field and the current are related by Maxwell's equation for the magnetic field flux

$$\oint \mathbf{E} \cdot d\mathbf{l} = -j\omega\Phi_z = -j\omega L I_z \Delta z. \tag{11}$$

A contour l shown in Fig. 3(b) has the length Δz (it may be arbitrary) and width equal to the WM half-period $a/2$. In (11), Φ_z is the magnetic flux through the area of this contour, and L is the collective inductance of a WM per unit length, taking into account the interaction of the reference wire with all the others. This parameter is assumed to be the same as L previously calculated for a PEC WM in [52], where the formula $L = \mu_0/abk_p^2$ was derived. This assumption is justified, because the absolute value of Z_w is small. Namely, we may apply the relation (10) for a WM of realistic wires, treating Z_w as $Z(\omega)$ and see that for copper, silver, aluminum and brass wires, the correction term in the right-hand side of this equation is negligibly small. The plasma frequency for realistic wires is the same as that for PEC wires. Therefore, the collective inductance also remains the same.

The integration in the left-hand side of Eq. (11) can be performed using the near-field approximation for the true field $E_z \approx -\nabla\varphi$, where φ is the electric potential created by all wires in the gap between the wires. The asymptotic integration in (11) for the infinitesimal interval $\Delta z = dz$ allows rewriting it in the form

$$Z_w I_z - \langle E_z \rangle + \frac{\varphi(z+dz) - \varphi(z)}{dz} = -j\omega L I_z. \tag{12}$$

Here $\langle E_z \rangle$ is the averaged value of E_z in the interval $x = [r_0, a/2]$ which is the same as the axial electric field averaged over the whole interval $x = [r_0, a - r_0]$ between the wires. The electric potential on the line ($x = a/2$, $y = 0$) — the dashed line in Fig. 3(b) — is denoted as $\varphi(z)$. The mean (macroscopic) electric field $\langle E_z \rangle$ in (12) arises not as an eigenwave amplitude, but as the result of the averaging of the microscopic axial field E_z over the interval between the adjacent wires. In Eq. (11), the microscopic field $E_z(a/2, 0, z)$ integrated over the interval Δz is used. On this line, E_z is adopted to be twice larger than the averaged field $\langle E_z \rangle$. Indeed, on the surfaces of both wires shown in Fig. 3(b), the axial component of the true electric field is almost equal to zero and increases with distance from the wire, so that its maximum $E_z(a/2, 0, z)$ is in the middle between these wires. The spatial variation of this field within the electromagnetically small interval $x = [r_0, a/2 - r_0]$ can be approximated as a linear one, which results in $\langle E_z \rangle = E_z(a/2, 0, z)/2$. The definition of the mean field via this arithmetic averaging of the true field differs from the classical one, which implies bulk integration of the true field over the unit cell volume. The last concept was adopted in the classical theory of natural media (see, e.g., [25]). The classical averaging for mean fields was used in the theory of bulk metamaterials composed of electromagnetically small particles (see [14]). This classical model considers only the near-field interaction between the elements. A homogenization model for an array of infinite realistic wires cannot be similar and uses another concept of the mean field — averaged over the interval between the adjacent wires.

Both the potential φ and current I_z introduced above result from the interaction of the reference wire with all other wires, where the far-field interaction is not neglected. The quasi-static formula for the true electric field $E_z \approx -\nabla\varphi$ expresses only the electromagnetic smallness of the period a.

The potential φ defined in the middle between two adjacent wires can be expressed via the microscopic linear charge density ρ distributed along the reference wire and the collective capacitance C of the WM per unit length. This capacitance is defined by the equation $C\varphi(z) = \rho(0, 0, z)$. The relation for C was derived in [52], which also showed that for the wires located in free space, $LC = \varepsilon_0\mu_0$.

Since ρ is related with I_z by the continuity equation

$$j\omega\rho(z) = -\frac{\partial I_z}{\partial z} = jq_z I_z(z), \tag{13}$$

the axial wavenumber q_z arises in our derivations. From (12) and (13), a pair of telegrapher-like equations relating $\varphi(z)$ with $\langle E_z \rangle(z)$ and $I_z(z)$ was obtained in [69]. Removing φ from this system, one obtains

$$\langle E_z \rangle = \left(j\omega L + Z_w + \frac{q_z^2}{j\omega C} \right) I_z. \tag{14}$$

This is the relation for the collective impedance of a homogenized simple WM. It differs from its PEC analogue by the term Z_w, and the formula for the effective permittivity of a simple WM (generalizing the result (2) to the lossy case) follows from it. Thus, the complex amplitude of the averaged field $\langle E_z \rangle$ introduced in the lossy WM model is physically the same as the eigenmode complex amplitude used in the lossless model. The axial wave number q_z and collective parameters L and C in (14) include the impact of electromagnetic interaction of the reference wire with all other wires of the WM.

To derive the effective permittivity from Eq. (14), the current I_z defined for the reference wire and the potential φ defined in the middle between the reference wire and its neighbor should be interpolated to replace the current density $J_z(0,0,z) \equiv I_z/ab$ and the potential $\varphi(a/2,0,z)$ with continuous functions defined in the entire space. Since the reference wire is chosen arbitrarily, any wire can be called the reference one. The function $I_z(z)$ defined on the discrete lines $(x = ma,\, y = nb)$ and the function $\varphi(z)$ defined on the discrete lines $(x = ma + a/2,\, y = nb)$ are extended, resulting in continuous functions $I(x,y,z) \equiv abJ(x,y,z)$ (where J is now the mean current density) and $\varphi_w(x,y,z)$. The extended potential $\varphi_w(x,y,z)$ was called the *additional potential of a WM* in [69]. The additional potential $\varphi_w(x,y,z)$ is not included in (14) and therefore does not affect the effective permittivity; we will discuss its role below in the context of the power flux. To obtain ε_{zz}, we only need to substitute the line current I_z in Eq. (14) by the mean current $I(x,y,z)$. Then, we may introduce the axial electric displacement $D_z = \varepsilon_0 \langle E_z \rangle + P$, where $P(x,y,z) = I(x,y,z))/j\omega ab$ is the axial polarization (density) of the homogenized medium. Combining the relation

$$D \equiv \varepsilon_0 \varepsilon_{zz} \langle E_z \rangle = \varepsilon_0 \langle E_z \rangle + \frac{I}{j\omega ab}$$

with Eq. (14), in which I_z is replaced by I, and taking into account that $L = \mu_0/abk_p^2$, we obtain the effective axial permittivity in the form:

$$\varepsilon_{zz}(\omega, q_z) = 1 - \frac{k_p^2}{k^2 - jkZ_w\sqrt{C/L} - q_z^2}. \qquad (15)$$

Relation (15) reduces to formula (2) in the special case $Z_w = 0$, i.e., for PEC wires. The transverse permittivity remains equal to ε_0.

If the wire radius r_0 is much larger than the skin depth, then for highly conducting wires (copper, silver, aluminum, brass), the dispersion equation (5) yields virtually the same dispersion diagram as that calculated for PEC wires. At 1–10 GHz for copper wires of radius $r_0 = (0.2\text{–}0.5)$ mm and WM period $a = 2\text{–}5$ mm, the absolute value of the dimensionless parameter $Z_w/\omega L$ has the order of 10^{-3}. The imaginary part of q_z at frequencies lower than the plasma one is proportional to ξ. Therefore, the decay factor $\mathrm{Im}(q_z)$ becomes smaller than the real part of q_z (which practically equals to k) by 3 orders of magnitude. The same applies to the ratio $\langle E_z \rangle / \langle E_t \rangle$, where $\langle E_t \rangle$ is the amplitude of the mean transverse electric field. For the transverse magnetic field, the model results in $\langle H_z \rangle = 0$. Such eigenwaves are called *quasi-TEM waves*. These waves substitute the non-uniform TEM waves propagating in a perfect WM at frequencies below ω_p and represent the special case of TM waves.

Note that in full-wave simulations, the low-frequency waves propagating along z are quasi-TEM ones even for WM of PEC wires. The reason is the impact of the transverse polarization of the wires by the electric field of the eigenmode. This polarization distorts the electric field distribution between the wires and results in $\langle E_z \rangle \neq 0$, although the microscopic field E_z nullifies on the surface of every wire.

However, in the framework of the homogenization model, we treat *these* quasi-TEM modes as TEM ones, because in the homogenization model, the electromagnetic interaction of the wires is considered as that of linear currents. The approximation of TEM modes is justified for low-frequency eigenwaves propagating along the PEC wires, because the longitudinal component is negligible compared to the transverse component. Meanwhile, mode decay, even comparably smaller than the wave number, cannot be neglected. Microwave WM endoscopes (see Subsection 4.5) have lengths of several λ, and neglecting the decay of quasi-TEM waves in them may result in noticeable errors. The same is true for WM resonators.

The result (15) can be generalized to the case when wires are both imperfectly conducting and periodically loaded with a small period D. In this case, the axial permittivity takes the form:

$$\varepsilon_{zz}(\omega, q_z) = 1 - \frac{k_p^2}{k^2 - jk\left[Z_w + Z(\omega)\right]\sqrt{\frac{C}{L} - \frac{\varepsilon_0\mu_0}{LC}q_z^2}}. \qquad (16)$$

Here, the plasma wavenumber should be modified in accordance with (10), and, since formula $k_p^2 = \mu_0/abL$ remains valid, L should be modified accordingly. Formula (16) can be easily generalized for wires hosted by a dielectric by replacing ε_0 by $\varepsilon_0\varepsilon_{\text{host}}$ in this relation and in the expressions for L, C, and Z_w.

2.4. Epsilon-Negative Wires

In 2002, the experimental results by Smith's group [63] proving the existence of left-handed metamaterials were disputed by Pokrovsky and Efros in [75]. They have shown that the near-field interaction of a wire lattice with an SRR lattice does not allow the effective permeability of the metamaterial to be negative. Therefore, these authors proposed to reconsider the full-wave numerical simulations and the measurements of the wave refraction beyond the concept of left-handed metamaterials. Ref. [75] was immediately criticized by many opponents. Ref. [76] explained that the near-field interaction for SRRs located in the middle between the wires is much weaker than the far-field interaction, which was neglected in the quasi-static homogenization model of [75]. Next, in 2003, a dynamic homogenization model of the Pendry-Smith left-handed metamaterial (which confirmed its negative permeability and negative refractive index) was presented in [77]. Motivated by this discussion, Pokrovsky and Efros suggested an alternative analytical model of a WM made of non-PEC wires accounting for these far-field

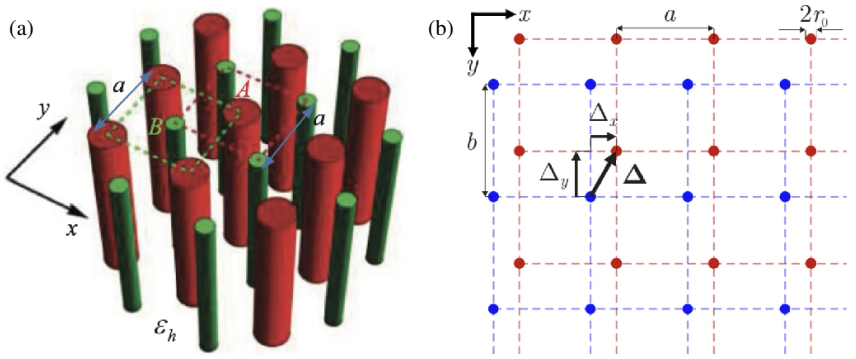

FIGURE 4. Nested WM geometries. Figures are taken from: (a) [81], (b) [82], both with the permission of publishers.

interactions [78, 79]. Their results significantly differed from those of [48] due to two reasons.

First, they used a different physical model of a metal wire. In [78, 79], in the complex permittivity of the wire material $\varepsilon_w = \varepsilon'_w - j\varepsilon''_w$, the authors neglected the imaginary part and assumed that $\varepsilon_w = 1 - \Omega_p^2/\omega^2$, where Ω_p was the Drude electron plasma frequency of a metal. In [78, 79], such lossless wires supported self-resonant collective oscillations of the charge density propagating along the z axis (the so-called *Langmuir waves*). In the model adopted in [78, 79], these collective plasma oscillations occur well below Ω_p. In fact, these oscillations are impossible in any realistic microwave WM, because the factor neglected in these works is not negligible; moreover, it is dominating, because $\varepsilon''_w \gg \varepsilon'_w$ for all metals in the microwave range.

The second issue of these two works was an approximation for the far-field interaction of wires disputed in [51]. An alternative model of a simple WM of thin cylinders with arbitrary permittivity ε_{cyl} was developed in this work similarly to that of [48]. It resulted in the following axial component of the permittivity tensor:

$$\frac{\varepsilon_{zz}(\omega, q_z, \varepsilon_{\text{cyl}})}{\varepsilon_{\text{host}}} = 1 + \left(\frac{ab}{(\varepsilon_{\text{cyl}} + 1)\pi r_0} - \frac{\varepsilon_{\text{host}} \left(\frac{\omega}{c}\right)^2 - q_z^2}{k_p^2} \right)^{-1}. \tag{17}$$

Unlike the expressions obtained in [78, 79], this relation yields formula (2) in the limiting case $|\varepsilon_{\text{cyl}}| \to \infty$.

2.5. Insulated Wires

In [80], a simple WM of bilayer wires is considered. The PEC wires of radius R_1 are enclosed in cylindrical tubes of outer radius R_2, whose permittivity is ε_1. In general, this permittivity may be complex, and the special case $\text{Im}(\varepsilon_1) = 0$ corresponds to insulated wires. The host medium permittivity (denoted above as $\varepsilon_{\text{host}}$) was denoted as ε_2. The approximation of thin wires $R_2 \leq 0.1a$ was used, and the lattice was assumed to be square ($a = b$). In this model, the transverse permittivity $\varepsilon_\perp \equiv \varepsilon_{xx,yy}$ cannot be approximated as ε_2, except for the case of very thin wires $R_2 \ll 0.1a$. The formula for $\varepsilon_\perp$ is as follows:

$$\varepsilon_\perp = \varepsilon_2 + 2\varepsilon_2 \left[f_V^{-1} \frac{(\varepsilon_1 + \varepsilon_2)R_2^2 + (\varepsilon_1 - \varepsilon_2)R_1^2}{(\varepsilon_1 + \varepsilon_2)R_1^2 + (\varepsilon_1 - \varepsilon_2)R_2^2} - 1 \right]^{-1},$$

where $f_V = \pi R_2^2/a^2$ is the volume fraction of insulated wires. When $R_2 < 0.1a$, the transverse permittivity approaches ε_2 and achieves it when $f_V \to 0$.

The formula for the axial permittivity *in our notations* takes the form:

$$\varepsilon_{zz} = \varepsilon_2 + \left[\frac{abk_1^2}{2\pi} \frac{\ln^2(R_1/R_2)}{\varepsilon_1 \ln(R_1/R_2) + (\varepsilon_1 - \varepsilon_2)k_1^2 R_2^2/2} - \frac{k_2^2}{\varepsilon_2 k_p^2} \right]^{-1},$$

where $k_{1,2} = \sqrt{k^2\varepsilon_{1,2} - q_z^2}$ and $k = \omega/c$ is the free space wave number, as above. In the limiting case $R_1 = R_2$, this formula transforms into (2). The formula for the plasma wave number k_p if $b = a$ is:

$$k_p^2 \approx \frac{2\pi/a^2}{\ln \frac{a}{2\pi R_2} + 0.527},$$

i.e., it corresponds to the substitution $b = a$ and $r_0 = R_2$ into formula (3).

2.6. Nested Wire Media

Simple WM with a unit cell $a \times b$ hosting two wires with different radii r_{01} and r_{02} shifted by a vector $\vec{\Delta}$ with respect to each other are called nested WM, see Figs. 4(a) and 4(b). Nested WM of PEC wires were studied in [81], where this terminology was introduced. The nonlocal effective permittivity tensor was derived in this paper, and the strong coupling between two parallel wire arrays was demonstrated. The macroscopic spatially dispersive response of the nested WM can be interpreted using an equivalent drift-diffusion model, where two different species of effective charge carriers contribute to the total current density (or medium polarization). For a given transverse component of the wave number $\mathbf{q}$, three eigenmodes exist in such a nested WM of PEC wires: two TEM modes and one

TM mode. A more general nested array composed of N parallel wire lattices can support N different TEM modes (in the lossy case — quasi-TEM modes). The plasma frequency for TM modes of nested WM can be tuned by varying the vector of shift $\vec{\Delta}$ [82], which can be used for the creation of mechanically tunable resonators for axion detection — see Subsection 5.4 for more details.

2.7. Power Flux and Energy Density in Simple Wire Media

The usual form of electromagnetic power flux density (the Poynting vector **S**), which is $\mathbf{S} = \mathbf{E} \times \mathbf{H}$ in the time domain and $\mathbf{S} = \mathrm{Re}(\mathbf{E} \times \mathbf{H}^*)/2)$ in terms of complex amplitudes, is no longer valid for media with spatial dispersion [83]. The same is true for the well-known expression for the electromagnetic energy density in a non-dispersive dielectric, which in the time domain is as follows:

$$W = \varepsilon_0 \frac{\varepsilon_{\text{host}} E^2}{2} + \mu_0 \frac{H^2}{2}.$$

For complex amplitudes, the denominator 2 is replaced by 4.

In the classical course of theoretical physics by Landau and Lifshits [25], this relation was generalized only for the case of temporal (frequency) dispersion. The case of spatial (wave vector) dispersion was not considered. Up to now, there is no general theory for the vector **S** and scalar W in materials with strong spatial dispersion; this problem has been studied only for materials with weak spatial dispersion. The expressions for the Poynting vector and the energy density derived in the lossless approximation for the so-called excitonic semiconductors illuminated by near-infrared or visible light can be found in [73, 83]. Other manifestations of weak spatial dispersion are the chirality of natural media, bianisotropy of composite media (metamaterials), and artificial magnetism. These effects arise in materials formed by small complex-shape particles. Bianisotropy is the local dependence of the electric polarization on the magnetic field and vice versa, the magnetic polarization on the electric field. Chirality is a special case of bianisotropy when both electric and magnetic polarizations of a medium are parallel. In cases of artificial magnetism and/or bianisotropy, the impact of the spatial dispersion of the effective permittivity on the Poynting vector and energy density reduces to the impact of the temporal dispersion of three material parameters — the so-called *reduced permittivity tensor* (in it, the dependence of the effective permittivity on the wave vector **q** is removed), the permeability tensor, and the *tensor of magneto-electric coupling*, which is called *chirality* in chiral media. The last two parameters originate from the spatially dispersive permittivity and do not depend on **q**. This theory is presented in Chapter 1 of [14].

As for the impact of *strong* spatial dispersion on the power flux and energy density, to our knowledge, the only work on WM, where these parameters were found, is [84], dedicated to a simple WM. To derive the expressions for **S** and W, two auxiliary problems of radiation of elementary sources were considered. In the first problem, the radiation is created by an axially polarized elementary source — a point electric dipole oriented along z, located in the middle between two adjacent wires. In the second problem, which is mathematically simpler, one of the wires of the WM is excited by an inserted lumped voltage source, whereas all other wires remain passive. In both cases, all currents flow along z, which allows the radiated field to be expressed via one scalar function, denoted in this work as Φ. This function is the same as vector potential, because in both problems, the vector potential has only a z-component. For both problems, the Fourier spectrum $\Phi(\mathbf{q})$ of this function was found in the closed form. Since it was not clear whether a homogenization model can be applied for WM excited by internal sources, $\Phi(\mathbf{q})$ was calculated beyond the homogenization model. The only approximation was the line current model for wires. The problem was solved via 3D Fourier expansion of an auxiliary source — δ-function of external current in one problem and δ-function of external electric field in the other problem. The result obtained for the function $\Phi(\mathbf{q})$ is not very important, and we do not reproduce it here. What is important is the coincidence of the solutions obtained for two radiation problems. The same result for Φ allowed the authors of [84] to claim that an electromagnetically dense lattice of thin wires is an effectively continuous material even in the problem of internal source radiation. Then the general approach of [69] was applied, and the power flux and energy density were expressed through macroscopic electric **E** and magnetic **H** fields, the extended current $I(x, y, z) = abJ(x, y, z)$, and the additional potential $\varphi_w(x, y, z)$ [84]. The result for the energy density in the frequency domain is as follows:

$$W = \varepsilon_0 \frac{\varepsilon_{\text{host}} E^2}{4} + \mu_0 \frac{H^2}{4} + C \frac{\varphi_w^2}{4ab} + L_{\text{tot}} \frac{I^2}{4ab}. \qquad (18)$$

Here, E and H are the absolute values of the complex amplitudes of the mean electric and magnetic fields. Note that in the homogenization model, we used brackets for the mean axial electric field to stress its difference from the true one. Here we do not discuss the true fields, and we do not need brackets. In (18), $L_{\text{tot}} = L + L_{\text{kin}}$ is the sum of the effective inductance per unit length of the WM and the kinetic inductance per unit length of an individual metal wire. L_{kin} becomes important in the THz range, whereas at microwaves, $L_{\text{kin}} \ll L$. Finally, φ_w and I are the complex amplitudes of the additional potential and mean current. The mean current can be expressed through the effective permittivity, because $I(x, y, z) = abJ(x, y, z) = j\omega abP(x, y, z)$, where $P \equiv P_z = \varepsilon_0(\varepsilon_{zz} - 1)E_z$ is the complex amplitude of the WM bulk polarization. However, the value of φ_w cannot be found via effective permittivity for realistic wires. To find φ_w, we should solve the system of telegrapher's equations obtained in [69].

The result for the Poynting vector also comprises this parameter. In the frequency domain, we have:

$$\mathbf{S} = \frac{1}{2} \mathrm{Re} \left(\mathbf{E} \times \mathbf{H}^* + \frac{\varphi_w I^*}{ab} \hat{\mathbf{z}} \right). \qquad (19)$$

We may avoid solving the telegrapher's equations only in one special case. For a simple WM of PEC wires located in free space, one of telegrapher's equations from [69] becomes very simple:

$$\varphi_w = -\frac{1}{j\omega C} \frac{\partial I}{\partial z} = ab \frac{q_z P}{C}.$$

Combining this equation with Maxwell's equations and the material equation $D_z = \varepsilon_0 \varepsilon_{zz} E_z$, the authors of [84] derived the relation

$$\frac{\varphi_w I^*}{2ab} = \frac{\varepsilon_0 \omega E^2}{4} \frac{\partial \varepsilon_{zz}}{\partial q_z}. \tag{20}$$

With the substitution of (20), the Poynting vector given by (19) is expressed solely via the mean fields and effective permittivity. The energy density in the case of PEC wires in free space can also be presented without φ_w [84]. For low frequencies $\omega < \omega_p$, the corresponding formula for W is especially simple:

$$W = \frac{\varepsilon_0 E^2}{2} \left(1 + \frac{q_x^2 + q_y^2}{k_p^2}\right).$$

In this formula, the magnetic eigenmode amplitude is expressed via the electric one, using the impedance of a TEM wave $\eta = E/H = \sqrt{\mu_0/\varepsilon_0}$.

3. COMPLEX WIRE MEDIA

3.1. Double Non-Connected Wire Medium

A double non-connected WM was first proposed in 1998 in [45] as a possible realization of biaxial negative epsilon in a solid metamaterial. Propagation orthogonal to both mutually perpendicular arrays of parallel wires was considered, and the nonlocality of the electromagnetic response was not revealed. In 2004, a more general analytical study [49] considered two rectangular arrays of parallel PEC wires with the same periodicity $(a \times b)$, oriented along the x- and y-axes and offset by $a/2$ in the z-direction. This structure corresponds to Fig. 1(c) when $d = b$.

The key features of this wire array were unveiled using the local field approach to find an eigenwave with wave vector $\mathbf{q}$. The derivations are similar to those of [48] (but slightly more difficult). According to [49], the tensor of spatially dispersive effective permittivity has the form:

$$\bar{\bar{\varepsilon}}_{\text{double}} = \varepsilon_{xx} \hat{\mathbf{u}}_x \hat{\mathbf{u}}_x + \varepsilon_{yy} \hat{\mathbf{u}}_y \hat{\mathbf{u}}_y + \varepsilon_{\text{host}} \hat{\mathbf{u}}_z \hat{\mathbf{u}}_z, \tag{21}$$

where ε_{xx} and ε_{yy} can be calculated using formula (2), with plasma frequencies $k_p(b, d, r_x)$ and $k_p(a, d, r_y)$ (see Fig. 1(c)) calculated using (3), respectively. This seeming absence of mutual interaction between the constituent simple WM results from structural symmetry — the wires of the second simple WM are located exactly in the middle between the wires of the first one.

The dispersion equation of this double WM (5), after substituting Eq. (21), dividing by k_{host}^2, and multiplying by $(k_{\text{host}}^2 - q_x^2)(k_{\text{host}}^2 - q_y^2)$, yields:

$$\prod_{m \in \{x,y\}} \left(k_{\text{host}}^2 - q_m^2\right) \left[k_{\text{host}}^2 - \left(k_p^{(m)}\right)^2 - q^2\right] - \left(k_p^{(x)} k_p^{(y)} q_x q_y\right)^2 = 0, \tag{22}$$

where $k_p^{(x)} = k_p(b, d, r_x)$ and $k_p^{(y)} = k_p(a, d, r_y)$, according to Fig. 1(c).

In general case, two arrays separated by a half-period gap may have different periodicity ($b \times d$ and $a \times d$). They may also be composed of wires with different radii (r_x and r_y), as illustrated in Figs. 1(c)–(d). However, the most studied configuration of a double wire medium (see [86–90]) is that with $a = b = d$ and identical wires in both arrays ($r_x = r_y = r_0$, i.e., $k_p^{(x)} = k_p^{(y)} = k_p$). This unit cell is shown in Fig. 5(a). In this case, Eq. (22) reduces to:

$$\left(k_{\text{host}}^2 - q_x^2\right)\left(k_{\text{host}}^2 - q_y^2\right)\left[k_{\text{host}}^2 - k_p^2 - q^2\right]^2 = k_p^4 q_x^2 q_y^2. \tag{23}$$

Using this model, the dispersion of a double wire medium can be examined graphically by plotting isofrequency surfaces and contours.

Below the plasma frequency, two modes propagating in the xy plane (parallel to the wires) exist. Typical isofrequency surfaces of these modes are shown for $k/k_p = 0.5$ in Fig. 5(b). The mode with a hyperboloid isofrequency surface is TM-polarized. The projections of the electric field on the x or y axis are substantial for some propagation directions. Such eigenmodes cannot exist in a simple WM. In a double WM that is not a multiwire transmission line even below the plasma frequency, they can exist. The projection of the true (microscopic) electric field on the axes of wires vanishes on their surfaces, but the same projection averaged over the medium unit cell is nonzero. In the q_x, q_y plane, the isofrequency of this mode is hyperbolic with asymptotes $q_x = \pm k$ and $q_y = \pm k$, as seen in Figs. 5(e)–(f). This hyperbolic mode is present across a wide frequency band and exists even above the plasma frequency. Ref. [91] showed that these modes arise as a peculiarity of the spatial dispersion in double WM, which is not the same as in the other hyperbolic metamaterials.

The second extraordinary mode, which is closer to the Γ-point in Fig. 5(b), is TE-polarized. For the in-plane propagation, its magnetic vector lies in the xy plane, and the electric field is along z. Its isofrequency surface in the $q_x q_y$ plane for $q_z = 0$ is close to that of the host medium (see Fig. 5(e)). However, in the diagonal plane, isofrequency contours for this mode are not circles, but super-quadric contours (solid curve in Fig. 5(g)). Therefore, this mode is not a TEM wave. An ordinary TEM wave with electric field along z, which does not "see" the wires, is not shown in our figure. Extraordinary low-frequency modes were thoroughly studied (analytically, numerically, and experimentally) in [90, 93].

At frequencies close to the plasma frequency and above it, additional modes appear, whose isofrequencies are centered at the Γ-point. They have ellipsoidal isofrequencies, typical for uniaxial dielectrics, as shown in Figs. 5(c)–(d). However, in a usual uniaxial dielectric, all ellipsoids corresponding to different frequencies are conformal. In a double WM, there are two types of isofrequency ellipsoids, and at every frequency, two ellipsoids intersect. Respectively, in the plane $q_z = 0$, the isofrequency contours are two crossing ellipses (dashed red lines at low wave numbers $q_{x,y}/k_p < 1$ in Fig. 5(e)). Even in the diagonal plane $q_x = q_y$, these modes (see n Fig. 5(g)) do not degenerate into those of a usual uniaxial dielectric. The polarization of these modes (most probably, hybrid ones), to our knowledge, has not been studied yet.

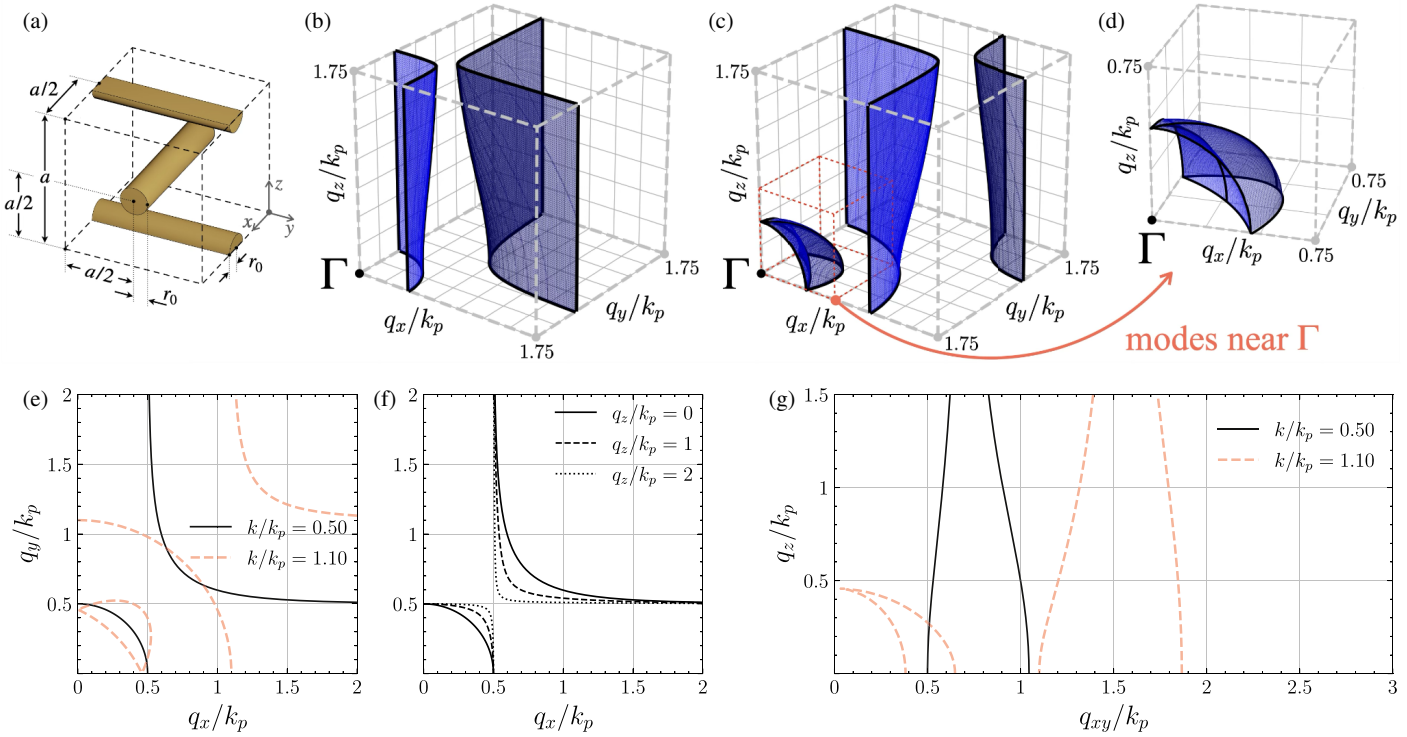

FIGURE 5. (a) Cubic unit cell of the most studied configuration of a double (non-connected) wire medium. Isofrequency surfaces are plotted from the effective medium model (22) in the first quadrant for (b) $k/k_p = 0.5$ and (c) $k/k_p = 1.1$. The enlarged surface near Γ point, which appears above k_p, is shown in (d). Isofrequency contours in $q_z = 0$ plane are shown in (e). (f) demonstrates isofrequency contours in different $q_x q_y$ planes for $k/k_p = 0.5$. Isofrequency contours in diagonal plane ($q_x = q_y$) are shown in (g). Subfigure (a) was taken from [85] with the permission of publishers. All plots were simulated by the authors of this review.

To conclude this section, we should make two notes about a double WM. First, the two arrays composing a double WM are not necessary offset by exactly a half-period in the z-direction, as in Fig. 1(c). In [86], even a special parameter describing the general offset of two parallel arrays forming a double WM was introduced. Unfortunately, the impact of its variation was not analyzed, and related physical effects have not need revealed. Second, the two arrays are not obliged to be perpendicular to one another. They may form an arbitrary angle, and the effects related to the variation of this angle may be interesting. For example, for the so-called moirè hyperbolic metasurfaces, with crossing grids of golden strips [94] or graphene strips [95], and stacks of twisted optical metasurfaces [96], new optical effects were revealed in the infrared and visible ranges [97]. The corresponding aspects of double WM remain underexplored (not only at microwaves), though they have a significant potential for future research.

3.2. Triple Disconnected Wire Medium

The addition of a third, non-intersecting array of parallel wires to a double non-connected WM creates a triple disconnected wire medium. To the best of our knowledge, this metamaterial was first proposed in [45]. However, in that work, its electromagnetic response was not studied, and this WM was only expected to have the electromagnetic properties of isotropic plasma in the microwave range.

The most studied arrangement of triple non-connected WM (see, e.g., in [45, 50, 92, 98]) consists of three mutually orthogonal and identical arrays of parallel wires, each comprising wires of the same radius r_0 forming a square lattice with period a. This structure has a cubic unit cell, shown in Fig. 6(a). In this case, the distance between adjacent mutually perpendicular wires is equal to $a/2$. A more general and less studied version, with different periods in all directions, is illustrated in Fig. 1(e). Similar to double disconnected WM (for which, after [49], all studies concentrated on mutually orthogonal lattices of parallel wires), the case of non-perpendicular triple WM remains unexplored.

Ref. [49] showed that in a triple non-connected WM, the effective permittivity tensor takes the form

$$\overline{\overline{\varepsilon}}_{\text{triple}} = \varepsilon_{xx}\hat{\mathbf{u}}_x\hat{\mathbf{u}}_x + \varepsilon_{yy}\hat{\mathbf{u}}_y\hat{\mathbf{u}}_y + \varepsilon_{zz}\hat{\mathbf{u}}_z\hat{\mathbf{u}}_z, \tag{24}$$

where all three components of the effective permittivity tensor are spatially dispersive. It was assumed that ε_{mm} ($m = x, y, z$) can be calculated using Eq. (2) after substituting the lattice periods and wire radius for the corresponding array. For the most studied arrangement (a cubic unit cell, $\varepsilon_{xx} = \varepsilon_{yy} = \varepsilon_{zz}$), this assumption was proven in [50].

Substituting the general tensor (24) into Eq. (5), multiplying by $(k_{\text{host}}^2 - q^2)\prod_m (k_{\text{host}}^2 - q_m^2)$, and dividing by k_{host}^2, results in [49]:

$$\prod_{m\in\{x,y,z\}} (k_{\text{host}}^2 - q_m^2)\left[k_{\text{host}}^2 - \left(k_p^{(m)}\right)^2 - q^2\right]$$

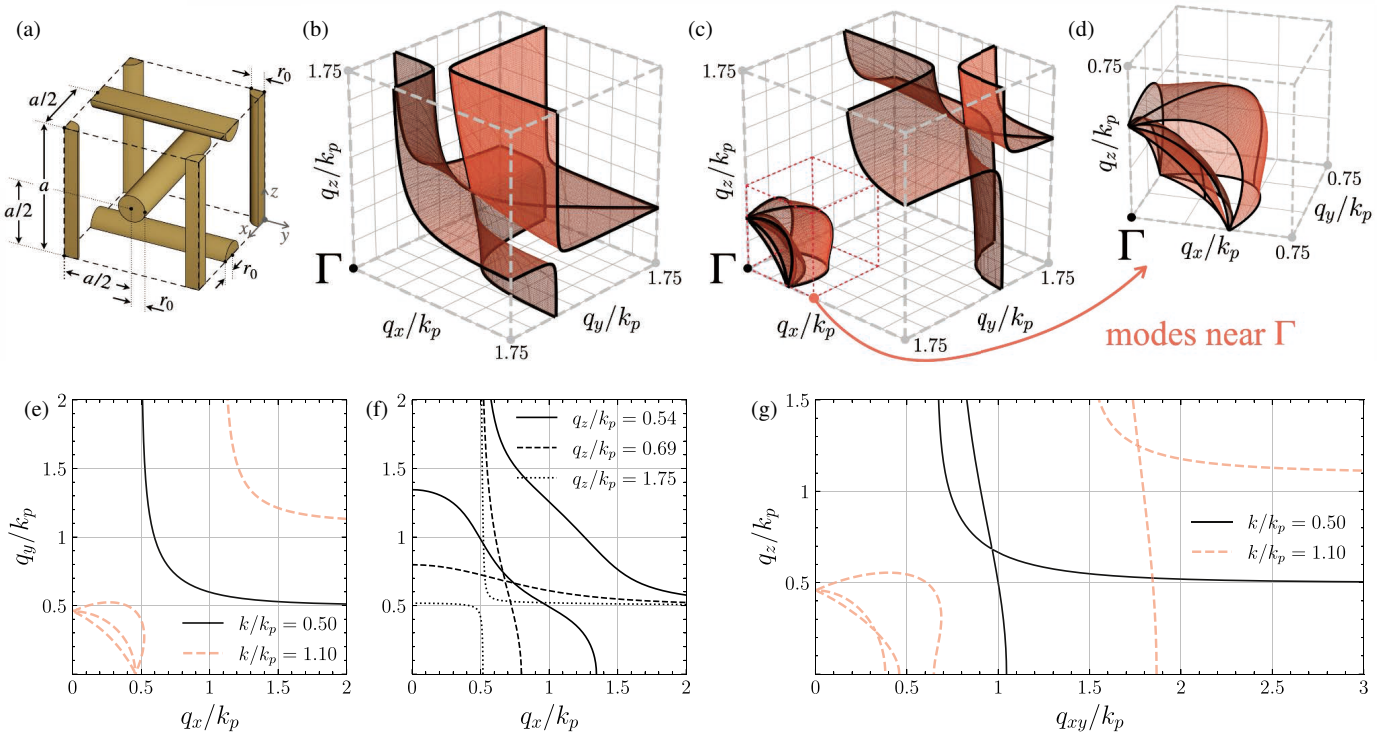

FIGURE 6. (a) Cubic unit cell of the most studied configuration of a triple (non-connected) wire medium. Isofrequency surfaces are plotted from the effective medium model (25) in the first quadrant for normalized frequencies (b) $k/k_p = 0.5$ and (c) $k/k_p = 1.1$. The enlarged surface near Γ point, which appears above k_p, is shown in (d). Isofrequency contours in $q_z = 0$ plane corresponding to two normalized frequencies are shown in (e). (f) shows isofrequency contours in different planes of the wave vector for $k/k_p = 0.5$. Isofrequency contours in the diagonal plane ($q_x = q_y$) are shown in (g). (a) was taken from [92] with the permission of publishers. Other plots were simulated for this overview.

$$- \sum_{m\in\{x,y,z\}} \left\{ \left(k_{\text{host}}^2 - q_m^2\right) \left[k_{\text{host}}^2 - \left(k_p^{(m)}\right)^2 - q^2\right] \right.$$

$$\left. \times \prod_{n\neq m} \left(q_n k_p^{(n)}\right)^2 \right\} + 2 \prod_{m\in\{x,y,z\}} \left(q_m k_p^{(m)}\right)^2 = 0.$$

For a cubic unit cell (see Fig. 6(a)), when $k_p^{(m)} = k_p$ for all $m = x, y, z$, this equation is simplified [92]:

$$\left(k_{\text{host}}^2 - k_p^2 - q^2\right)^3 \left(k_{\text{host}}^4 + \frac{1}{2}\left(q^4 - \sum_m q_m^4\right)\right)$$

$$+ \left(k_{\text{host}}^2 - k_p^2 - q^2\right) \left[\left(k_{\text{host}}^2 - 2k_p^2 - q^2\right) \prod_m \left(q^2 - q_m^2\right)\right.$$

$$\left. - \frac{k_p^4}{2}\left(q^4 - \sum_m q_m^4\right)\right] + 2k_p^4 (q_x q_y q_z)^2 = 0. \qquad (25)$$

This dispersion equation is simple enough to analyze the dispersion properties of the triple non-connected WM analytically, as it was done in [50, 92], and to plot isofrequency surfaces in reciprocal space. These surfaces are shown in Figs. 6(b)–(d).

Work [92] rigorously proved that below the plasma frequency, a triple non-connected wire medium possesses four characteristic directions, in which the phase velocities of all eigenwaves are equivalent. Even for a the slightest deviation from these directions, noticeable birefringence occurs. These directions are the optic axes of the WM. They are oriented along the four main diagonals of the cubic unit cell (see Figs. 6(b) and (g)). For all of them, the so-called conical refraction [99, 100], with a triangular cross section of the refraction cone, was observed in numerical simulations in [92].

This metamaterial also exhibits hyperbolic isofrequency contours in the $q_x q_y$, $q_y q_z$, and $q_x q_z$ planes below the plasma frequency, shown in Figs. 6(e)–(f). The hyperbolic shape of isofrequencies, whose features can be engineered by varying mutual locations of the parallel arrays and their periods, can become the basis for many potential physical effects, such as those discussed above for double WM.

Above the plasma frequency, the metamaterial supports five modes, depicted in Fig. 6(c). A short analytical treatment of these modes can be found in [50]. However, publications focusing on the high-frequency eigenmodes of triple non-connected WM remain scarce. In general, electromagnetic properties of a triple WM remain underexplored.

3.3. Connected Triple Wire Medium

Connected topology of a triple WM, illustrated in Figs. 1(g)–(h), was first introduced by Rotman in 1962 in [42], but the discussions and the analysis of this structure started only three decades later. A similar structure (originally referred to as the

scaffold structure) composed of thin dielectric rods was investigated in [101] as a material providing broad photonic bandgaps. In late 1990s, a connected structure of metal wires attracted the attention of researchers [44, 102, 103] as an analogue of isotropic plasma possessing a 3D low-frequency bandgap.

Two pioneering studies [44, 103] independently investigated triple WM with a connected topology. In [103], Sievenpiper and co-authors studied a wire-mesh photonic crystal with a diamond-like geometry and numerically calculated and experimentally verified its dispersion diagram. Pendry et al. [44] analyzed a WM introduced in [42], whose cubic unit cell is shown in Fig. 1(g).

In the present work, we focus on the latter configuration, because the theoretical studies of the diamond geometry are insufficient (in [103], the polarization of eigenmodes was not studied, and no further studies in this area are available). Meanwhile, the cubic configuration of triple connected WM is well investigated in the literature.

The plasma model of this metamaterial, in which the plasma frequency was defined as the low-frequency cutoff, was proposed in [44]. In accordance with this work, the permittivity $\varepsilon_{\text{eff}} \equiv \varepsilon_{xx} = \varepsilon_{yy} = \varepsilon_{zz}$ is as follows:

$$\varepsilon_{\text{eff}}(\omega) = 1 - \frac{\omega_p^2}{\omega\left[\omega + j\frac{\varepsilon_0}{\sigma\pi r_0^2}(\omega_p a)^2\right]}, \tag{26}$$

$$\omega_p^2(a, r_0) = \frac{2\pi c^2}{a^2 \ln(a/r_0)},$$

where σ is the conductivity of the metal (with wires in free space). This result was derived neglecting the far-field interaction of the wires (no spatial dispersion) and using the concept of plasmons in WM; very thin wires are required for the model to be valid [45]. Thus, the wire radius was $r_0 \sim 1$ μm, which is not relevant for microwave WM of any realistic metal.

A non-contradictory homogenization of such a connected WM for arbitrary propagation direction of an eigenwave was developed in [50]. The following effective permittivity tensor for PEC wires in free space was derived:

$$\bar{\bar{\varepsilon}}_{\text{connected}} = \bar{\bar{\mathbf{I}}} - \frac{k_p^2}{k^2}\left(\bar{\bar{\mathbf{I}}} - \frac{\mathbf{qq}}{q^2 - l_0 k^2}\right). \tag{27}$$

Here, the dyadic form $\mathbf{qq}$ corresponds to the wave vector $\mathbf{q}$, and $l_0 = 3\kappa^2/(\kappa^2 + 2k_p^2)$ is a factor characterizing the connected topology. The parameter κ was defined in [50] as:

$$\kappa^{-2} = \left(\frac{a}{2\pi}\right)^2 \sum_{n\neq 0}\left[\frac{J_0(2\pi n r_0/a)}{n}\right]^2, \tag{28}$$

where J_0 is a Bessel function. Eq. (27) uses an approximate relation for the plasma frequency derived in [48].

Unlike the previously considered WM, for a connected WM, the effective permittivity tensor is not diagonal. We can rewrite it in a form with separated tangential and longitudinal components, standard for optically isotropic but spatially dispersive materials with a center of symmetry [25, 73, 104]:

$$\bar{\bar{\varepsilon}} = \varepsilon_t(\omega)\left(\bar{\bar{\mathbf{I}}} - \frac{\mathbf{qq}}{q^2}\right) + \varepsilon_l(\omega, q)\frac{\mathbf{qq}}{q^2}, \tag{29}$$

where ε_t and ε_l are the transverse and longitudinal permittivities, respectively. For PEC wires ($|\varepsilon_{\text{rods}}| \to \infty$), they take the form:

$$\varepsilon_t(\omega) = 1 - \frac{k_p^2}{k^2}, \tag{30}$$

$$\varepsilon_l(\omega, q) = 1 + \frac{l_0 k_p^2}{q^2 - l_0 k^2}, \tag{31}$$

where the transverse plane and longitudinal direction are determined by the direction of propagation and not by the optical axis of the material.

Equation (5) allows identifying the degenerate TEM mode [50, 105]:

$$k^2 = k_p^2 + q^2 \tag{32}$$

as well as the longitudinal mode with dispersion:

$$k^2 = k_p^2 + \frac{q^2}{l_0} = k_p^2 + \frac{\kappa^2 + 2k_p^2}{3\kappa^2}\, q^2. \tag{33}$$

These modes are shown in Fig. 7, where they correspond to frequencies (normalized to c/a) in the range 0.4–0.6. The lowest branch corresponds to a longitudinally polarized mode. In [106], the authors demonstrated that these analytical predictions closely match numerical simulations near the plasma frequency for a connected wire medium with thin wires ($a/r_0 = 100$). In that case, the assumption $\kappa \gg k_p$ simplifies the longitudinal mode dispersion to $k^2 = k_p^2 + q^2/3$.

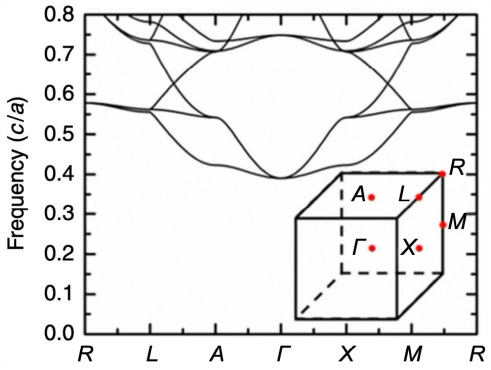

FIGURE 7. Dispersion diagram for a connected wire medium. Coordinates of the high symmetry points in the reciprocal space are $\Gamma = (0,0,0)^{\text{T}}$, $\text{X} = (\pi/a, 0, 0)^{\text{T}}$, $\text{M} = (\pi/a, \pi/a, 0)^{\text{T}}$, $\text{R} = (\pi/a, \pi/a, \pi/a)^{\text{T}}$, $\text{L} = (\pi/a, 0, \pi/a)^{\text{T}}$, $\text{A} = (0, 0, \pi/a)^{\text{T}}$, where a is a period of a cubic geometry. Adopted from [107] with the permission of publishers.

To conclude this section, let us once again make two remarks. First, connected double WM (a parallel set of rectangular wire meshes with subwavelength cells) have not been studied at all. However, this type of WM hardly deserves attention. The microwave response of square wire meshes, and their transmissive

and reflective properties are well known (see, e.g., [29]). At frequencies where the cell size is smaller than $\lambda/2$, this mesh is almost fully reflecting; therefore, such a WM is opaque and does not support extraordinary eigenwaves. Only at higher frequencies, where a double connected WM becomes a metallic photonic crystal, nontrivial effects arise, including backward wave phenomenon and negative refraction [108–115]. These effects are beyond the scope of the present paper.

The second remark concerns connected triple WM and disconnected double and triple WM, which are rich in physical effects, already revealed and potentially expected ones. Here, the unexplored area is much broader than the explored one. For example, none of the available works on these metamaterials raise the fundamental question of electromagnetic energy and power flux in them. Thus, the existing theory of double and triple WM is very insufficient. The same can be said about the interlaced WM reviewed below.

3.4. Interlaced Wire Medium

The idea of nested WM generalized to connected triple WM is called *interlaced wire media*. It consists of two (see Fig. 8(a)) or more (see Fig. 8(c)) connected triple WM, inserted into one another without crossing (no electrical contact between triple WM). This structure was proposed in [116], which also comprised a model representing it as an effective network of circuits. Unfortunately, this model was heuristic, not scientifically grounded, and the derived equations proved to be incompatible with Maxwell's equations. This point was noticed by the authors and even reflected in the paper title (where the suggested

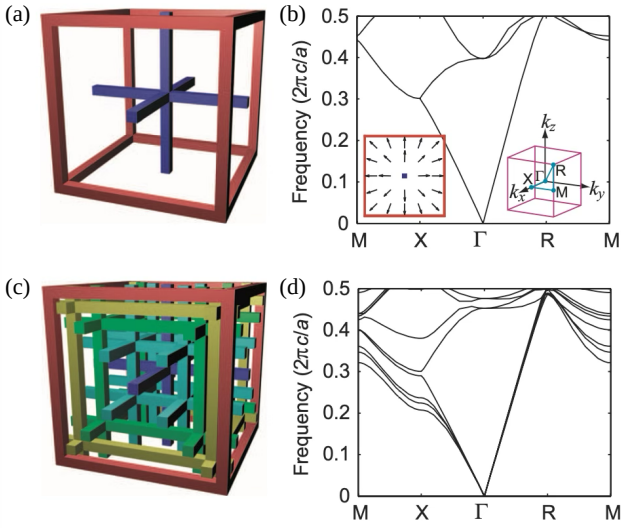

FIGURE 8. Examples of interlaced WM. (a) A single cubic unit cell of a two-network structure. (b) The band diagram for the two-network example. (c) A five-network cubic structure example. Each network has metal wires along the x, y, and z directions. For the i^{th} network, these wires meet at $(\pm x_i, \pm x_i, \pm x_i)^{\text{T}}$ in the cubic unit cell, where x_i's chosen to be 0, $a/12$, $3a/16$, $a/3$, and $a/2$. (d) The band diagram for the five-network example. Coordinates of the high symmetry points in the reciprocal space are $\Gamma = (0,0,0)^{\text{T}}$, $\text{X} = (\pi/a, 0, 0)^{\text{T}}$, $\text{M} = (\pi/a, \pi/a, 0)^{\text{T}}$, $\text{R} = (\pi/a, \pi/a, \pi/a)^{\text{T}}$, where a is a period of cubic geometries. Figures are taken from [116] with the permission of publishers.

metamaterial was called non-Maxwellian). However, the authors claimed that this contradiction compromises Maxwell's equations rather than their model. Fortunately, in later works on this subject such as [117–120], where the terminology of interlaced WM was introduced, there is no controversy, and all results are physical. These works investigated only interlaced WM consisting of two connected triple WM (see Fig. 8(a)).

As [119] noted, all intertwining regular arrays of wires whose constituent lattices are not electrically connected can be called interlaced WM. However, interlaced WM more complex than the double ones (see Figs. 8(c)–(d)) have not been studied yet, to our knowledge. Therefore, in this section, we discuss only the double interlaced WM depicted in Figs. 1(i), (j) and Fig. 8(a).

An analytical model of the effective permittivity tensor of a double interlaced WM was suggested for the first time in [121]. This homogenization model utilized the results obtained for a triple connected WM in [50, 104]. Only the symmetric case was considered, where the distance between adjacent wires of two lattices was $a/2$ (with the shift vector $\mathbf{s} = (0.5, 0.5, 0.5)^T a$, as shown in Fig. 9). This restriction was applied to minimize the coupling between two constituent WM, similarly to [49], where the electromagnetic response of a double WM with symmetric arrangement of two parallel arrays was found to be equal to the combination of the responses of two simple WM. For an interlaced WM, the two responses of triple connected WM given by (30) and (31) can be additively combined. Unlike [49], in the present case, the permittivity tensor components are defined not with respect to the coordinate axes, but with respect to the propagation direction [121]:

$$\varepsilon_t(\omega) = 1 - \sum_{i=A,B} \frac{k_{p,i}^2}{k^2} \tag{34}$$

$$\varepsilon_l(\omega, q) = 1 + \sum_{i=A,B} \frac{l_{0,i} k_{p,i}^2}{q^2 - l_{0,i} k^2} \tag{35}$$

where $k_{p,i}$ is the effective plasma wavenumber for the ith lattice ($i = A, B$), and $l_{0,i}$ is a dimensionless slow wave factor that determines the strength of the nonlocal response (see, e.g., [50, 104]). This *connected topology factor* arises in Eq. (27) and was introduced in [50].

In [117], a layer of this WM illuminated by a plane wave was studied. The effect of resonant extraordinary transmission was found (with both analytical model and full-wave simulations) at a specific, quite large incidence angle and interpreted as angularly selective tunneling. The polarization-insensitive resonances of the transmittance are periodically repeated over the frequency axis, i.e., can be referred to as the Fabry-Perot ones. However, they can be observed only within a very narrow angular range.

In [119], low-frequency eigenmode dispersion was studied, and longitudinal mode polarization was revealed. This polarization makes this low-frequency eigenwave an analogue of a bulk plasmon (a longitudinal eigenwave that exists in isotropic plasma and in metals in the ultraviolet range [74]). Ref. [122] proposed to control this plasmon dispersion by an affine deformation of the structure. In [120], bound states in the continuum

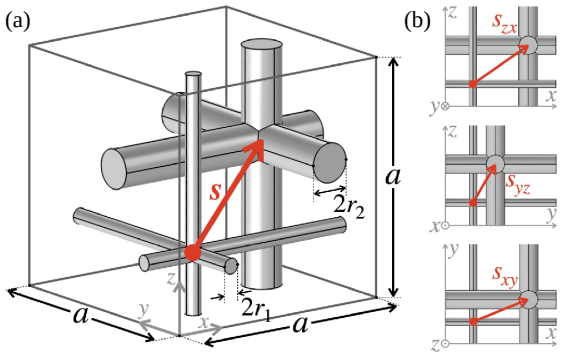

FIGURE 9. Unit cell of a generalized double interlaced wire medium. Two cubic lattices have the same periodicity a, but different wire radii (r_1 and r_2). The shift vector $\mathbf{s}$ is formed by three vectors $\mathbf{s}_{zx}$, $\mathbf{s}_{yz}$, and $\mathbf{s}_{xy}$.

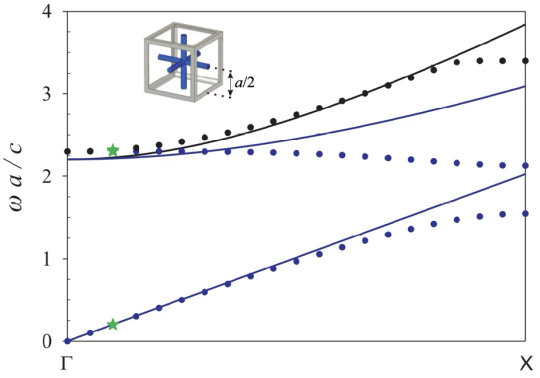

FIGURE 10. Dispersion along ΓX — theory versus numerical results. The host dielectric is free space, and the wire radii are $r_1 = 0.001a$ for mesh A and $r_2 = 0.05a$ for mesh B. Figure is taken from [117], reproduced with the permission of publishers.

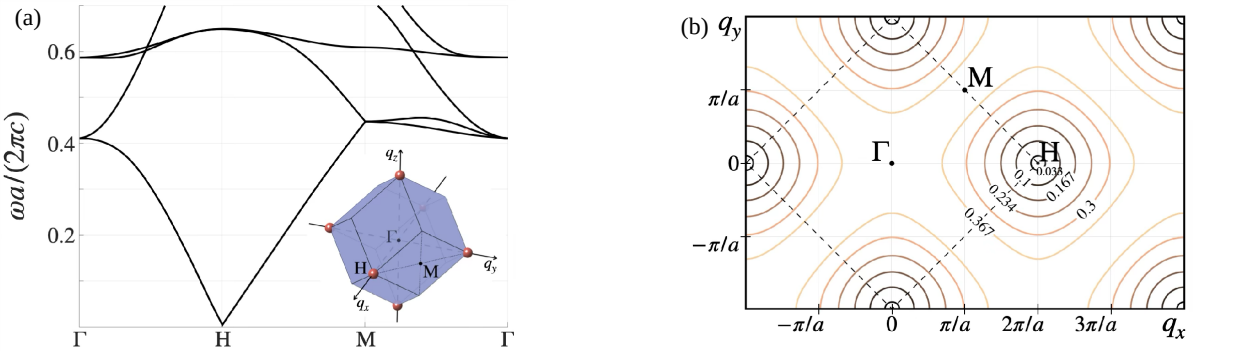

FIGURE 11. (a) Wave dispersion along the wave vector path ΓHMΓ for a body-centered cubic configuration of a double interlaced WM. (b) Isofrequency contours in the q_xq_y plane. Figures are taken from [119] with the permission of publishers.

(BIC) were found. In all the mentioned works, the analytical model of the symmetric interlaced WM was validated by numerical simulations.

Even for a double interlaced wire medium composed of two simple cubic lattices of the same periodicity, studied in the works mentioned above, there are some parameters whose variation may offer new physical effects. As Fig. 9 shows, these parameters may be (1) distance between two lattices given by the vector $\mathbf{s}$, (2) wire radii in both lattices r_i ($i = 1, 2$), and (3) wire materials and cross-section shapes in two lattices. The point (3) has not been investigated at all. In all the available works, interlaced WM of PEC wires were considered. Meanwhile, the impact of parameters $\mathbf{s}$ (point (1)), and r_i (point (2)) was studied.

The dispersion of the longitudinal modes of a double interlaced wire medium follows from the dispersion equation of an effective plasma $\varepsilon_l(\omega, q) = 0$ [119]. For different wire radii in lattices ($r_1 \neq r_2$), this equation reduces to a quadratic equation in q^2, resulting in two longitudinal modes, see Fig. 10. The transverse mode, which is also plotted in the figure, is obtained by solving equation $q^2 = (\omega/c)^2\varepsilon_t(\omega)$. Mode polarization was verified in [117] numerically.

For identical lattices ($r_1 = r_2$) and maximal distance between the lattices (i.e., the offset vector $\mathbf{s}$ components equal to $a/2$), the structure unit cell becomes a body-centered cubic one [119]. This symmetric metamaterial configuration is a special case when longitudinal eigenwaves with small effective wavelength are excited at low frequencies. The point at which the lowest longitudinal mode arises moves to the corner of the Brillouin zone, corresponding to the primitive unit cell of the WM lattice (see Figs. 9(b) and 11).

Periodicity in the low-frequency limit ($\omega \to 0$) means that isofrequency surfaces emerge from a set of points in the reciprocal space, noticeably shifted with respect to the Γ point [107].

Isofrequency contours for this body-centered configuration calculated in the k_xk_y plane are shown in Fig. 11(b). Ref. [123] discusses the opportunities of control of this long-wavelength eigenwave, not considered [122].

When the body-centered cubic symmetry is disrupted — by displacing the sub-lattices from their symmetric configuration, or by employing sub-lattices composed of wires with different radii, or, finally, through a combination of both, the low-frequency point shifts back to the center of the Brillouin zone [107] (see Fig. 8(b)). For such asymmetric configurations with a diagonal relative offset of lattices ($\mathbf{s} = (1, 1, 1)^T d$) and different wire radii ($r_1 \neq r_2$), a special analytical model for the slope coefficient of the lowest longitudinal mode was proposed in [120]. This model is equivalent to a hydrodynamic model of

a two-fluid ideal warm plasma, see, e.g., in [124]. This plasma model gives a linear approximation of the lowest mode — *electron acoustic waves*:

$$\omega_a^2 = \frac{m^2 + (\kappa_2/\kappa_1)^2}{m^2+1}\,\kappa_1^2 c^2 q_a^2. \tag{36}$$

Here, $m = \omega_p^{(2)}/\omega_p^{(1)}$, q_a is the wave vector of the acoustic wave in the metamaterial, and κ_i ($i = 1, 2$) are dimensionless thermal pressure parameters (κ_i have nothing in common with κ in Eq. (28)), mainly determined by the connectivity of the wires.

The wire-mesh pressure parameter was found to be in the range $[2/3, 3/4]$ for $r/a \in [10^{-2}, 0.2]$ and $\kappa \to 1/\sqrt{3}$ in the limit of small radii. For identical lattices composed of thin wires ($r/a < 10^{-2}$), the dispersion of fundamental electron acoustic waves mode can be approximated as $k_a \sim q_a/\sqrt{3}$. The authors of [120] claimed that this theory is valid for a large variety of configurations and concluded that the electron acoustic waves in a double interlaced WM have quasi-longitudinal polarization. The dispersion equation derived in that work generalizes that of the symmetric model and weakly depends on particular geometrical parameters of WM.

4. BOUNDARY PROBLEMS FOR WIRE MEDIA

In real applications, WM cannot be infinite — they are bounded. Their theory would be useless if it was not applicable for boundary problems with WM. All homogenization models of WM reviewed above have been obtained from first principles of electrodynamics. Therefore, they result in non-mesoscopic formulas for the effective medium permittivity — i.e., they remain valid for spatially bounded WM. However, spatial dispersion makes the effective permittivity difficult to use in boundary problems. Indeed, consider a plane wave incident on a WM interface from outside (e.g., free space). The tangential component of the wave vector $\mathbf{q}$ of the wave refracted into WM is preserved (as follows from Maxwell's boundary conditions). The normal component of the wave vector should be found from the dispersion equation of the corresponding infinite WM. However, spatial dispersion offers more than one real solution for $\mathbf{q}$ with given tangential components of this vector at a given frequency. In this situation, the medium polarization (or induced current density) cannot be found only from Maxwell's boundary conditions and the dispersion equation. The effective permittivity included in Maxwell's boundary conditions via $\mathbf{D}$ relates the mean electric field with the mean polarization vector only for one eigenwave, not for their set. To find the relation between the amplitudes of two or more excited eigenwaves, we need additional boundary conditions (ABCs). This problem for spatially dispersive media was understood long ago and solved for excitonic semiconductors illuminated by visible or infrared light in [83, 125]. In this case, together with usual refracted waves, an *exciton wave* arises and propagates very slowly together with expansion of strongly coupled electron-hole pairs (also called excitons in the theory of photoelectricity).

ABCs may be needed even when an only eigenmode is excited by the incident wave, because in some media (even with weak spatial dispersion), polaritons (see above) may be efficiently excited on the surface. Recall that polaritons are imaginary (or even complex) solutions of a dispersion equation in a medium. In natural media, polaritons excited on the interface have negligibly small amplitudes. However, in most regular metamaterials, the maximal lattice period (though it is subwavelength in the operation band) is comparable with λ. It may enable a significant amplitude of one or more dominant polaritons, and neglecting it can yield a noticeable mistake in the solution of boundary problems for metamaterials (see the discussion in Chapter 10 of [14]).

For lattices of electromagnetically small inclusions with periods not larger than $a \sim (0.1\text{–}0.2)\lambda$, the boundary problem can be solved without ABCs — via introducing a transition layer on the metamaterial interface (see Chapter 11 of [14]). Across this layer, the material parameters (permittivity and permeability) linearly vary from their bulk values to unity (free space values). Alternatively, one may introduce a transition metasurface, which is a compressed version of a transition layer [126].

However, for WM, this approach is unsuitable, since in their homogenization models, the constituents are infinitely long. Therefore, for each type of WM, one should derive and use ABCs.

4.1. Additional Boundary Conditions for Simple Wire Media

For a simple WM, the interface parallel to the z axis is not a problem (see, e.g., Chapter 3 of [15]). One should properly locate this interface (half-period from the outer wires) and apply the Maxwell boundary conditions. In this case, high-amplitude polaritons and multiple eigenmodes are not excited if q_z is fixed. In the problem of internal reflection from this interface, ABCs are also not needed. However, if the interface is tilted or orthogonal to the wire axis (i.e., to the z axis), ABCs are necessary.

For a lossless semi-infinite simple WM with an orthogonal interface at $z = 0$, ABCs were introduced in [127]. In this case, a TM-polarized polariton can be excited with an amplitude comparable to that of the TEM mode. To relate the amplitudes of two excited modes (an eigenwave and a polariton), we need only one simple equation: at the ends of thin wires, their currents are zero. This gives the boundary condition for the mean current density $J(z = 0) = 0$, which may be expressed as a combination of two eigenmodes — one TEM and one TM (polariton). This simplest ABC allows solving the reflection and refraction problems. This approach was generalized to a half-space filled with tilted wires in [128].

In our opinion, the key work on ABCs for simple WM is [31], analyzing two types of the orthogonal interface between WM shown in Fig. 12. In Fig. 12(a), at the interface between two WM with different wire radii (one radius r_2 is larger than the other r_1), thin metal patches are introduced. If $r_1 \to 0$, the left WM vanishes, and we obtain a mushroom metasurface mentioned in Introduction. Since 1999, these metasurfaces have been used as artificial magnetic walls. A conventional magnetic wall is a plane in free space at a distance $h = \lambda/4$ from a metal plane. Mushroom metasurface with the thickness $h = \lambda/40$ allows reducing the magnetic reflector thickness by an order of

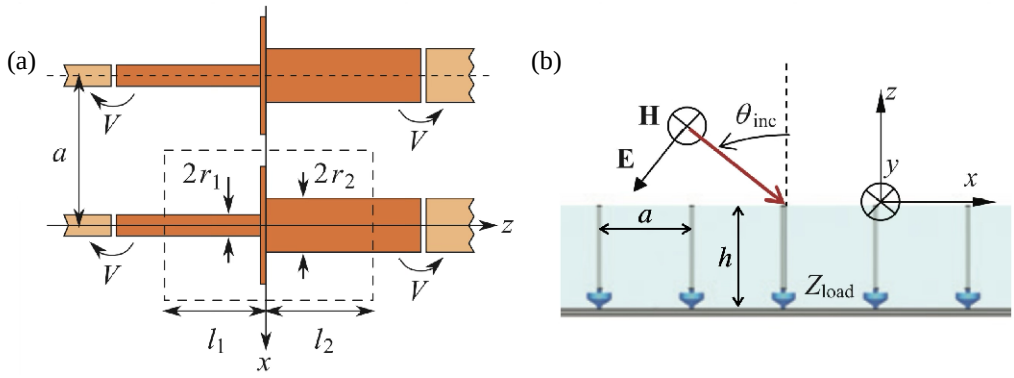

FIGURE 12. Two important types of a simple WM interface. (a) The case when $r_1 \to 0$ corresponds to mushroom metasurface. (b) The top and bottom interfaces demand different ABCs. Figures are taken from [31] with the permission of publishers.

magnitude [28]. In Fig. 12(b), at the top interface, the wires simply end, and at the bottom interface, they are connected to the ground via lumped loads. This WM interface can be used in intelligent surfaces — reconfigurable anomalous reflectors, which consume very low power needed for an electronic controller (which distributes the biasing voltages over the load array). Nowadays, these metasurfaces are considered a promising replacement for the relay stations for 5G and 6G telecommunications. In numerous works (see, e.g., [129–132]), tunable lumped loads — varactors or pin-diodes — connected to the ground as shown in Fig. 12(b) are used to vary the wave deflection from the mushroom metasurface. In this case, one type of ABCs is used for the top interface (the case shown in Fig. 12(a) with $r_1 = 0$), and another type of ABCs for the bottom interface (the case in Fig. 12(b)).

ABCs of both these types were derived in [31] using telegrapher's equations from [69], known properties of the patch grid (considered as a capacitive reflector for waves propagating in the WM), and the quasi-static analysis of a single interface. For the case in Fig. 12(a) (when $r_1 \to 0$), we need only one ABC for the current J_2 in wire medium 2:

$$J_2 + \chi \frac{\partial J_2}{\partial z} = 0, \tag{37}$$

where $\chi = C_{\text{tip}}/C$. Here, C is the collective capacitance per unit length of the WM (see above), and C_{tip} is the effective capacitance of the wire tip. For large patches and narrow gaps between them (the patch size is close to a), $C_{\text{tip}} = C_{\text{patch}}$ is the effective capacitance of the patch grid, related with its grid (or sheet) impedance as $Z_g = 1/j\omega C_{\text{patch}}$. In applied electrodynamics, the grid impedance is defined as $Z_g = E_t/J_s$ — the ratio of the tangential component E_t of the mean electric field in the plane of a planar grid of metal elements to the mean surface current J_s induced in this grid (see, e.g., in [29]).

Without patches, C_{tip} is the effective collective capacitance of the wire ends (tips). This value is not negligible, except for the case when r_2 is negligibly small compared to a. Indeed, the wires end with small, but not negligible metal patches of area πr_2^2. In other words, the interface of a simple WM is a capacitive grid even without patches. Only in the limiting case, when r_2/a is so small that $C_{\text{tip}}/C \ll 1$, $\chi \approx 0$ and Eq. (37) reduces to $J_2 \equiv J = 0$.

For the bottom interface at $z = -h$ in Fig. 12(b), the following ABCs were derived:

$$E_{x,y} = 0, \quad \frac{\partial J}{\partial z} - j\omega C Z'_{\text{load}} J = 0.$$

Here, the first equation is a trivial result of the ground presence. The lumped impedance Z'_{load} in the second equation takes into account the known parasitic inductance L' and capacitance C', which arise when a lumped, finite-size load with a proper impedance Z_{load} is inserted between a wire and a metal plane. In [31], the resulting impedance Z'_{load} takes the form

$$Z'_{\text{load}} = j\omega L' + \frac{1}{j\omega C' + Z_{\text{load}}^{-1}}.$$

Work [81] considered a slab of a nested WM (Fig. 4(a)) illuminated by a plane wave. One wire array was terminated on both sides by patches, and another one (with a smaller wire radius) had trivial terminations. It was assumed that ABCs with different parameters χ hold for these constitutive simple WM separately, i.e., $\chi = C_{\text{patch}}/C$ for the first wire array, and $\chi = 0$ for the second array. This assumption was confirmed by full-wave simulations. Though their ABCs are decoupled for large incident angles, the two arrays proved to be strongly electromagnetically coupled. This coupling enabled the interference of a narrow-band quadrupole-type resonance of the overall slab polarization and a broadband dipole-type resonance, which resulted in a Fano resonance of the transmission. This effect is interesting due to practical importance of the Fano resonance in all areas of applied electrodynamics, including microwaves [133].

4.2. Additional Boundary Conditions for Other Wire Media

Additional boundary conditions for a double non-connected WM, based on the vanishing of the current at the ends of very thin wires in the form $J(z = 0) = 0$ (where, as above, J is the mean current density along z, and $z = 0$ describes the interface plane), were heuristically introduced in [86]. In this work, one array of parallel wires was orthogonal to the interface, and the

other one parallel to it. Two mutually orthogonal wire arrays with wires at the angle 45° to the normal to the interface were considered in [134]. In [135], this result was generalized for the upper half-space having a complex isotropic permittivity of general type (covering the cases of dielectrics, metals, and non-excitonic semiconductors). Finally, in [136], ABCs were theoretically derived (Eq. (13)) for an arbitrary angle between the wires and the interface. We do not reproduce these long equations here, but we should stress that in this general case, one additional equation is not enough, because the frequency and the tangential component of the wave number determines two TE-polarized surface waves decaying into WM, but having noticeable amplitudes on the interface. Two ABCs together with the dispersion equation of a double WM allow finding all three relevant amplitudes. When the interface-wire angle is sufficiently close to 45°, the eigenmode has a very high refractive index, i.e., the refracted wave is significantly shortened compared to λ.

For a connected triple WM, ABCs were obtained in [104]. They were not derived; it was simply assumed that the product $\varepsilon_{\text{host}}E_z$ (here $E_z \equiv \langle E_z \rangle$ is the axial component of the mean electric field) is continuous across the interface $z = 0$ when one WM array is orthogonal to the interface and two others are parallel to it. This assumption was validated by full-wave numerical simulations of the transmission and reflection by a WM layer. Note that for very thin wires, there is no need to derive the mentioned ABC. Since $D_z = \varepsilon_0\varepsilon_{\text{host}}E_z + J/j\omega$, the continuity of $\varepsilon_{\text{host}}E_z$ across the plane $z = 0$ is nothing else but the above-discussed condition $J(z = 0) = 0$.

In [121], the ABC in the form $\partial J(z = -h))/\partial z = 0$ was obtained for a layer of triple connected WM of thickness h when one constitutive simple WM is orthogonal to the PEC plane (located at $z = -h$) and connected to it, and two other simple WM are parallel to the interfaces. Moreover, [121] showed that the ABCs introduced for a triple connected WM should also hold for an interlaced WM formed by two triple connected WM, at least when two constituents are symmetrically located and the interface is not tilted.

A tilted interface for triple connected WM was incorporated into the analytical model in [137], where ABCs were obtained for an arbitrary angle between the wires and the interface. These derivations used the approach suggested in [136]. This theory was experimentally confirmed in [137] by measuring the scattering of a plane wave by spherical samples of triple connected WM. In calculations, a WM sphere was modeled as an exotic sphere with many flat facets. ABCs were applied to all of them.

ABCs obtained for triple connected WM and applicable to double interlaced WM were used to study the low-frequency tunneling through a double interlaced WM slab [117] discussed above. ABCs for the surface of a triple connected WM modified by metallic antennas were heuristically introduced in [123, 138]. In a very recent paper [139], the authors developed a semi-analytical scattering theory that explained the strong impact of the WM surface terminations and the internal geometry on both resonance frequencies and quality factors of an interlaced WM slab operating as a Fabry-Perot resonator.

4.3. Surface Waves in Wire Media

Work [140] considers the reflection coefficient of a metal-backed slab of a simple WM illuminated by a TM-polarized plane wave. Their geometry corresponds to Fig. 12(b), where $Z_{\text{load}} = 0$, the slab thickness is denoted as L instead of h, and the host medium permittivity is ε_h. Above, we have already discussed this problem: it demands ABC $J = 0$ at the slab interface. At low frequencies $\omega < \omega_p$, this condition should be added to Maxwell's boundary conditions to find the ratio of the TEM eigenmode amplitudes to the polariton mode excited on the surface. Ref. [140] extends this theory to a complex wave vector of the incident wave, namely, with a tangential component $k_\parallel$ larger than k and imaginary k_z. In this case, the reflectance may turn to infinity, i.e., a wave decaying away from the interface of a lossless WM slab may exist in it without an incident wave. The condition of this reflection singularity can be written as the dispersion equation of this surface wave. In fact, Eq. (14) of [140] describes not only surface waves, but also guided TM-modes of a WM slab, and this equation is valid at all frequencies up to the photonic crystal band (in which $\omega \gg \omega_p$). At low frequencies ($\omega < \omega_p$), the solution of this equation describes the polariton of an unbounded WM. In the present case, it is called *surface plasmon polariton* (SPP), which is a proper surface wave, because it propagates in the tangential plane xy, and its field is localized on the WM slab surface. We briefly discussed such a polariton in Subsection 3.2. Below, we will discuss it in detail with an explicit example.

Maxwell's boundary conditions impose $q_\parallel = k_\parallel$, where $k_\parallel$ is a real number (larger than k). For SPP $q_\parallel > k_h$, where $k_h = k\sqrt{\varepsilon_h}$ is the wavenumber of the host dielectric (notice that in [140], different notations are used). Therefore, q_z is a large imaginary number describing the amplitude decay into the WM. Similarly, k_z describes the decay of this wave into free space. This WM polariton is a proper surface wave — its energy is localized on the interface of the slab. As explained in Subsection 3.1, TM-waves propagating along the wires of a simple WM at low frequencies are called plasmons. Thus, surface waves propagating along a WM slab below the plasma frequency can be correctly referred to as SPP waves. In the optical range, SPP waves are excited on smooth interfaces of gold or silver. These two metals have inductive surface impedance in a certain frequency band (in the visible range for interface with a semiconductor, and in the near ultraviolet range for a dielectric) [141]. This is true for all SPP waves — they exist only on inductive surfaces. Ref. [140] showed that in the SPP frequency band, the surface impedance of a microwave WM slab is inductive.

In Fig. 13, a dispersion diagram of TM-polarized modes guided along a WM slab is presented for three different ratios L/a (a is the WM period). TE-modes are not shown, because their field does not interact with the wires. These modes are formed by pairs of ordinary eigenwaves of the WM and are TE-modes of a metal-backed dielectric slab.

In Fig. 13, the horizontal axis corresponds to the normalized frequency $\omega_n = L/4\lambda_0\sqrt{\varepsilon_h}$ ($\lambda_0 \equiv \lambda$ in our notations). The normalized wave number of the mode denoted as $k_\parallel/\beta$ corresponds to the vertical axis; it can be called the wave shorten-

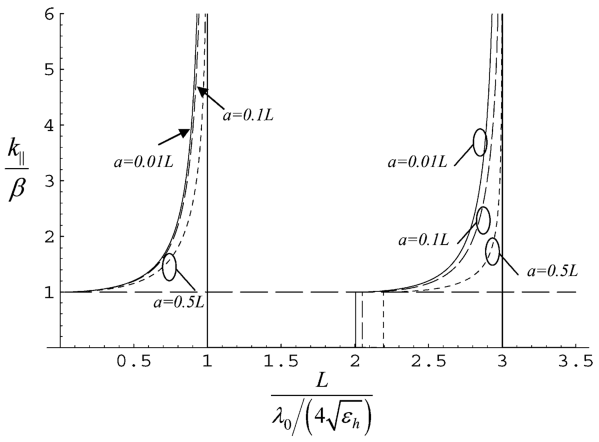

FIGURE 13. Dispersion diagram of TM-waves guided along a simple WM slab of thickness L with the host medium of permittivity ε_h on a PEC ground plate. Dispersion curves are calculated for three ratios of the WM period a to the slab thickness L. The light line of free space is indicated by the dashed line $k_\parallel/\beta = 1$. The asymptotes of SPP waves are vertical lines. Figure is taken from [140] with the permission of publishers.

ing coefficient or slow-wave factor, because in our notations, $\beta \equiv k$. In this example, the plasma frequency is engineered so that $\omega_p \approx 8\pi c\sqrt{\varepsilon_h}/L$, which means $\omega_n \approx \omega/\omega_p$.

The slab eigenmodes lie entirely above the free-space light line, i.e., they cannot propagate without decay along z in free space. The slab eigenmode in the range $\omega_n < 1$ is an SPP. It decays along z in both directions away from the slab surface.

In the band $\omega_p < \omega < 2\omega_p$, there are neither TM-polarized nor TE-polarized guided modes, because in a grounded dielectric slab, even TE-modes cannot exist. Therefore, the only TE-mode that has no cut-off (TE_0 mode) cannot be excited. The lowest guided mode is TE_1, characterized by a low-frequency cut-off, which in this case remains at $\omega \approx 2\omega_p$. In other words, Ref. [140] revealed that a grounded WM slab with a properly chosen thickness has a broad complete bandgap similar to a photonic crystal. Therefore, a WM slab may serve as a medium for a defect waveguide (see, e.g., [142]). In the range $2\omega_p < \omega < 3\omega_p$, besides TE-modes, a high-frequency SPP exists. The group velocity of both fundamental and high-frequency SPPs (the value inverse to the dispersion curve slope) tends to zero when $\omega \to \omega_p$ and $\omega \to 3\omega_p$, respectively. These important theoretical results were validated in [140, 143] not only numerically, but also experimentally.

The dispersion of guided modes of WM slabs (see Appendix in [144]) can be used for the development of metalenses [8, 9] capable of imaging with subwavelength resolution from the far-field; more details are available in Subsections 4.5 and 5.1.

Work [145] advanced the investigation of surface waves in a simple WM slab. First, the authors compared the theoretical predictions of the model [140], using spatially dispersive WM permittivity and ABCs, with the simplistic model of [45], neglecting the spatial dispersion and treating WM as an effective plasma. Second, in [145], a mushroom structure (wires terminated by patches on top) was considered and compared with the structure without patches. Third, besides guided modes of a WM slab, which have real $q_\parallel > k \equiv \beta$, leaky modes of the slab were considered: they have complex $q_\parallel$, which allows energy propagation into free space. Fourth, mushroom metasurfaces (mushroom structures with electromagnetically short wires $L \ll \lambda$) were compared with mushroom structures with long wires ($L \sim \lambda$). In [145], the simplistic model was shown to fail in most interesting scenarios, including both types of mushroom structure ($L \sim \lambda$ and $L \ll \lambda$). ABCs were revealed to be necessary for theoretical calculation of surface and leaky waves. Next, WM slabs were shown to support proper leaky waves that are backward (with oppositely directed phase and group velocities) and improper leaky waves that are forward (with co-directed phase and group velocities). These improper leaky waves are excited when the wires are terminated by patches, and the proper leaky waves are excited in the absence of patches. We will not discuss leaky waves in this subsection, because they are not equivalent to surface waves. Since excitation of leaky waves is a physical effect unusual for flat interfaces of effectively continuous media, leaky waves excited in a WM slab are discussed below in Subsection 5.3 together with other unusual effects theoretically revealed for WM.

4.4. Bound States in the Continuum

Bound states in the continuum (BICs) are non-radiating resonances of open systems that coexist with the continuum of radiative states at the same frequency, but are decoupled from this continuum [146–148]. First proposed in quantum mechanics, BICs arise from mechanisms such as symmetry protection or destructive interference, which prevent energy leakage of the modes despite their dispersion curves above the light line. Their exceptionally high Q-factors and strong field confinement have made BICs a powerful concept in various open systems, providing a rigorous framework for understanding and engineering resonances with ultra-low radiation losses.

BICs in bounded WM are a relatively new research direction, and only a simple WM and a double interlaced WM have been studied so far. Authors of [149] considered a plane wave with TEM polarization (with magnetic field along y and electric field having only x and z components — an oblique incidence) scattered on a simple WM slab, unbounded along the x and y axes and having a finite thickness in the z direction (see the axes in Fig. 1(a)). The effective medium model for PEC wires expressed by formula (1) was combined with ABCs [127] discussed above in Subsection 4.1. This slab supported two types of BICs: (1) symmetry-protected BICs, resulting from the polarization mismatch between longitudinal TEM waves propagating along the wires and ordinary TEM waves, which do not interact with the wires; and (2) accidental BICs, which arise due to the destructive interference between eigenwaves (TEM modes) and polaritons (TM modes) excited in the slab. For both types of BICs, analytical expressions for their spectral and angular properties were derived and validated by numerical simulations.

As discussed in Subsection 3.4, a double interlaced WM supports a low-frequency longitudinal mode [117, 119], which is difficult to excite directly from free space without modifying the WM boundaries [118]. The hydrodynamic plasma model

developed in [120] allowed the authors to approximate the frequencies of the symmetry-protected BICs observed in numerical simulations of the WM slab by the standing wave solution of electronic acoustic waves (36). BIC robustness against geometrical perturbations and symmetry breaking was numerically investigated. The authors of [120] claimed that BICs may exist even in cubic WM samples smaller than λ, which needs additional validations in addition to their simulation. The most recent study [139] investigates how different boundary terminations of interlaced WM affect the resonance frequencies and the corresponding quality factors, with modeling supported by experimental data.

4.5. Wire Media Resonators and Endoscopes

In the available literature, WM resonators are based on cylindrical samples of simple WM sandwiched between two metal planes [152] or (more often) enclosed into a rectangular metal box [82, 150, 153–155]. In both cases, we are interested in the fundamental resonance of the WM sample in the transverse (xy) plane. This resonance corresponds to the smallest electromagnetic size of the cavity cross-section. For a cubic box shown in Fig. 14(a), it holds when $d = \lambda/2$. Then, the electric field for three equivalent modes (TM_{101}, TM_{011} and TM_{110}) of the resonator becomes zero on every wall on which it is tangential. For both cubic and cylindrical resonators filled with WM, the properties of the excited fundamental quasi-TEM mode drastically change in case of mechanical deformations of the wires or dielectric present in the cavity. Resonance frequency shift and broadening of the resonance band enable efficient sensing of permittivity [156] and mechanical stress [152]. A more interesting physical effect is observed in WM resonators with WM engineered for this cavity resonance to form at frequencies slightly higher than ω_p; this effect will be discussed below in Subsection 5.4. Here, we discuss only the boundary problem for a sample of simple WM enclosed into a resonator. If the wires are well-connected to the bottom and top wall, the boundary problem becomes very simple for both open resonator of two parallel plates [156] and cavity [152].

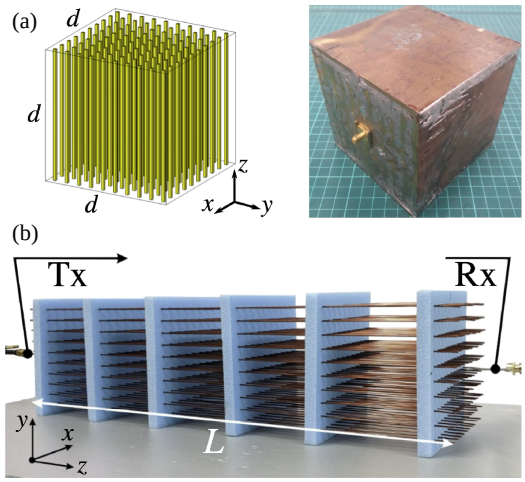

FIGURE 14. (a) Cubic cavity filled with WM. (b) A microwave WM endoscope. Here, Tx is a transmitter illuminating a planar object of small scatterers located in the left dielectric holder (not seen in this picture). Rx is a receiver (scanning probe measuring the transverse electric field amplitude). Figures are taken from: (a) [150], (b) [151], both with the permission of publishers.

Since all wires of the WM sample shown in Fig. 14(a)) are connected to two horizontal metal planes, we do not need ABCs to build an analytical model of the WM resonator. Instead, we may apply the mirror image principle, considering the metal (copper, aluminum, brass) of the cavity walls as a PEC. According to mirror imaging, a WM sample of length d is equivalent to a piece of an infinite WM endoscope of the same length. Wires connected to the PEC planes respond to the electromagnetic field as if they were infinitely long. The distance between the outer wires of the WM sample and the lateral walls of the closed cavity is either equal to $a/2$, as in Fig. 14(a), or larger, as in [155]. Therefore, ABCs are not needed for lateral surface of WM samples even for a closed cavity.

An example of a microwave WM endoscope is shown in Fig. 14(b). Modeling of this WM sample with open terminations seems to be impossible without ABCs. However, it is not true. As shown in [157], proper functionality of a WM endoscope is achieved at frequencies for which the wire length is equal to $D = m\lambda/2$ ($m = 1, 2, 3, ...$) — this is the condition of the Fabry-Perot transmission resonance, discussed and implemented in further works on WM endoscopes (see [18, 158–160]). Under this condition, ABC of a simple WM (in the form $J = 0$) holds at the endoscope ends $z = (0, D)$, automatically following from the effective medium model that implies the current distribution $J(x, y, z) = F(x, y) \cos q_z z$.

Indeed, WM endoscopes can operate only in narrow bands of Fabry-Perot resonances. Only one work [151] overcame this restriction, achieving broadband operation. However, in this case, ABCs were also not needed. Their structure included transversely polarized point scatterers located exactly in the middle between every four adjacent wires. In this case, and only in this case, an endoscope of parallel wires with a small period $a \ll \lambda$ operates not as a WM sample, but as an array of effective cables formed by these wire groups.

Thus, based on all available works on WM resonators and endoscopes, we may conclude that ABCs are not needed for modeling these structures, though they are necessary in many other boundary problems with WM, including metalenses [8, 9].

5. MAIN PHYSICAL EFFECTS IN MICROWAVE WIRE MEDIA

Above, we have reviewed the known theoretical models of microwave WM. This analytical modeling reveals the electromagnetic properties of WM, which enable some unique and useful physical effects, justifying the categorization of WM as metamaterials. In this section, we briefly review the main physical effects which make microwave WM very important metamaterials. We do not consider potential devices based on them, which deserve a separate review. We only mention some applications that evidently follow from these physical effects.

5.1. Subwavelength Imaging of Distant Objects

In a simple WM, at frequencies below ω_p, eigenwaves are nonuniform TEM waves for PEC wires and quasi-TEM waves for realistic wires, both propagating along z. We already mentioned that this effect allows calling WM metamaterials, and here, we discuss this point in more detail. The homogenization model does not restrict the transverse wave numbers q_x and q_y, but it is no longer applicable when the granularity of the medium (period a) exceeds the scale of the spatial oscillation. This results in the restriction $q_{x,y}^{\max} \approx \pi/a$. However, $a \ll \lambda$, which means that the spatial spectrum of the packet of TEM waves that can propagate in perfect WM may be very broad, extending far beyond the spatial spectrum of waves propagating in free space.

Consider a planar object of complex shape located at a subwavelength distance $h \ll \lambda$ from the interface $z = 0$ of a simple WM. When illuminated by microwave radiation, it creates a scattered field in the far zone and a near field, whose intensity repeats the subwavelength details of the object. This near field is created by waves with large transverse wave numbers $k_x^2 + k_y^2 > k^2$. Since in free space, $k_x^2 + k_y^2 + k_z^2 = k^2$, these waves are evanescent, i.e., they decay along z in free space. In other words, the subwavelength image of the object is a packet of evanescent waves. Since $h \ll \lambda$, this wave packet is still strong on the WM interface, where it is converted into a packet of quasi-TEM modes having the same spatial spectrum $q_{x,y} = k_{x,y}$. Therefore, the subwavelength image of the object is encoded in the spatial spectrum of the WM eigenwaves. Due to very low attenuation of quasi-TEM waves in WM, this image is transferred without distortions to electromagnetically large distances.

In [157, 161], this effect was called the *canalization of subwavelength images*. Numerous full-wave simulations and many experiments confirmed this theory for WM endoscopes operating in different frequency ranges. The corresponding experiments with microwave WM endoscopes were reported in [17, 18, 66, 144, 162–166]. Canalization of near-field imaging in a simple WM is a resonant effect. As discussed above, a Fabry-Perot resonance is necessary for the proper operation of a WM endoscope. Though in [151], the broadband subwavelength image of a microwave object was canalized, this work was not devoted to canalization in WM. As explained above, in that special case, the endoscope of parallel wires operated as an array of cables.

We should note that not only endoscopes of parallel wires may be used for subwavelength imaging. Ref. [134] revealed negative refraction in a double non-connected WM. The next work of the same group [167] theoretically explored a layer of this WM concentrating the transmitted field and revealed that unlike usual dielectrics, the double WM offers subwavelength concentration of the power of a spherical wave incident on the layer. Further, [168] theoretically and experimentally demonstrated that this layer is actually a near-field pseudo-lens, capable of producing images of planar objects with subwavelength resolution similar to a layer of left-handed metamaterial with $\varepsilon \approx \mu \approx -1$.

Another opportunity of subwavelength imaging at large distances from the source is provided by the so-called metalenses [8, 9]. These open WM resonators provide dramatically different scattering diagrams for multiple resonant modes with complex near-field distributions and closely packed resonant frequencies. These property allows reconstructing wideband near-field source profiles from the far-field measurements around the metalens. In contrast to other subwavelength imaging methods discussed in this subsection, this method does not operate at a single frequency and requires a wide frequency spectrum of the source.

5.2. Purcell Effect in Simple Wire Media

Historically, this effect was defined by Edward Purcell as the enhancement of an emitter's spontaneous emission decay rate when the emitter is introduced into an open cavity. In 2015, Ref. [169] generalized this effect as the enhancement of the decay rate due to a resonant passive scatterer (not necessary an open resonator) with which the emitter is coupled, and the emitter is not necessary inside the scatterer. That work means that the Purcell effect is not a quantum effect: it is the enhancement of the instantaneous value of the radiated power calculated or measured during the emission process. This enhancement arises due to the near-field coupling between the emitter and a passive scatterer with a resonant size. This insight into the Purcell effect was suggested a few months prior to [169] in [170], which noticed that the quantum emitter in the Purcell effect is fully analogous to a small active (transmitting) antenna, and the role of the enhancing cavity can be played by a resonant passive antenna (in the optical range, by a resonant silver or gold nanoparticle). A microwave example of the Purcell effect is the enhancement of the radiation of a short dipole antenna in a Yagi-Uda array. Ref. [171], also published in 2015, maximally generalized the Purcell effect as the enhancement of a radiation source (a classical antenna or a quantum emitter) coupled with any passive structure more favorable for radiation than free space. Nowadays, the Purcell factor F_P of a general structure is defined as the ratio of the power radiated by a given source in presence of a structure to the power radiated in its absence — when the source with the same dipole moment is located in free space.

If we apply this concept of the Purcell effect to the radiation of an axially polarized electric dipole located in a simple microwave WM, the Purcell effect becomes negative at $\omega < \omega_p$. In this range, the power radiated by an axial dipole is lower than that radiated in free space [84], i.e., $F_P < 1$. Physically, it happens because at low frequencies, the wires strongly screen the radiation of an axial dipole in all directions, except for the domain between four wires surrounding the dipole. However, in the middle of this domain, this radiation is absent, because the dipole does not radiate along its own axis, and the dipole pattern at very small angles is close to zero. However, as shown in [172], if the radiating dipole is orthogonal to the wires, the situation in the low-frequency range is the opposite.

Work [172] considered the radiation of an arbitrary oriented electric dipole located inside an unbounded simple WM beyond the homogenization model. The response of the lattice of paral-

lel wires with finite radius r_0, made of a material with arbitrary complex permittivity ε, was studied using the Bloch expansion of the total field and the 3D Fourier expansion of the external excitation (dipole field in free space). For the special case $r_0 \ll a \ll \lambda$ and $|\varepsilon_w| \gg 1$, an asymptotic (low-frequency) solution was obtained for the dyadic Green function $\overline{\overline{G}}$ of the WM (the dyadic Green function of a structure relates the electric field of a point electric dipole oscillating at a given frequency and interacting with the given structure to its dipole moment $\mathbf{p}$). At the location of the dipole $(x_0, y_0, z = 0)$, the real part of the Green function is infinite, but the imaginary part remains finite for most structures. In general case, the Purcell factor F_P is proportional to $\mathrm{Im}[\overline{\overline{G}}(x_0, y_0, 0)]$ (see e.g., [171]). For a dipole located exactly in the middle between four adjacent PEC wires and having $p_x = p_y$, the following approximate relation (here, presented in our notations) was derived:

$$F_P \approx \frac{3k_p^2}{8k^2} \ln\left(1 + \frac{4\pi}{k_p^2 a^2}\right).$$

At the frequency $\omega \approx \omega_p/2$, this formula gives $F_P \sim 100$, and at $\omega \approx 0.1\omega_p$, $F_P \sim 10^3$. If the dipole shifts from the middle point towards one of the wires and is normally oriented to it, F_P grows from about 10^3 to nearly 10^4. The physics underlying such a significant radiation growth is the excitation of a group of four nearest wires surrounding the source. Unlike the axial dipole, which does not radiate along z, this transverse dipole exhibits the radiation pattern maximum along the z axis. Moreover, the transverse dipole acts as an effective voltage exciting the nearest wires. Therefore, the source near field is efficiently converted into an eigenwave packet canalized along the wires. This wave packet is concentrated between four adjacent wires, forming an effective cable.

The same result was obtained in [172], also for transversely oriented magnetic dipoles. For axial electric dipoles, $F_P \ll 1$ at $\omega < \omega_p$ and $F_P \approx 1$ at $\omega > \omega_p$. These results agree with those obtained in [84] for the radiated power. For axial magnetic dipoles, the Purcell effect is absent ($F_P \approx 1$), because the electric field of these dipoles is orthogonal to the wires.

For a transverse dipole, the highest values of the Purcell factor (for the source located in the middle between the wires, $F_P \approx 10^3$ at $\omega \approx \omega_p/2$) were obtained for very large, but finite permittivity of the wires. This effect is related with the transverse resonances of an individual wire, which arise when $r_0\sqrt{|\varepsilon_w|}$ is of the order of λ. This regime was further elaborated for WM of polaritonic nanowires operating in the mid-infrared range (see, e.g., [173, 174]).

High Purcell factor for transversely polarized microwave scatterers forming an object enabled the high-intensity subwavelength image of this object, transmitted to and detected at a large distance from the object in [151].

5.3. Epsilon Near Zero: Super-Refraction

Consider an isotropic medium with the refractive index $n < 1$. If a wave passes from free space into this medium through a flat interface, then, in accordance with Snell's law, the angle of refraction is larger than the angle of incidence. If the wave passes from the medium into free space, the refraction angle is smaller than the incidence angle. If a radiation source located inside this medium creates a beam of divergent rays, all of them are refracted into free space with reduced angles to the normal to the interface compared to the angles of incidence. This phenomenon is known as *super-refraction*. In the case $n \ll 1$, the super-refraction results in the formation of a collimated (low-divergence) wave beam. Since for isotropic media $n^2 = \varepsilon$, this regime is called epsilon-near-zero (ENZ) one. The only natural ENZ medium with low losses is fully ionized low-density plasma at frequencies slightly higher than ω_p [74]. However, this medium is unstable, and engineering its resonance frequency to fall in the desired microwave range is extremely difficult. Therefore, authors of [175, 176] suggested using a simple WM instead of plasma. In accordance with Eq. (8), for TM-waves excited in a WM sample above the plasma frequency, the value $n = q/k_{\text{host}}^2 = \sqrt{1 - k_p^2/k_{\text{host}}^2}$ can closely approach zero. For refraction of a TM wave passing from a WM into free space, n plays the role of the refractive index.

If a single source creating TM-waves at a frequency satisfying $\omega \approx \omega_p$ and $\omega > \omega_p$ is located in a layer of simple WM, this layer may operate as a very compact collimator, making the radiation of a short dipole highly directive. The corresponding structure is depicted in Fig. 15(a). A proper choice of the layer thickness h and the height h_s of the dipole source above the metal (ground) plate allows reducing the internal reflections and creating a the beam with zenithal radiation, whose directivity is strongly enhanced compared to that of a dipole source in free space. Directivity enhancement was reported for a frequency band where $n < 1$ (from 4 to 6 GHz, whereas the plasma frequency is about 3.9 GHz). At 4.2 GHz, the interplay of super-refraction and resonant transmission resulted in a conical beam with an intensity maximum at $\theta = 18°$. For this conical beam, the highest directivity of radiation was obtained.

Work [176] aimed to efficiently excite the so-called *improper leaky wave* by a dipole source. In this case, the wires should be orthogonal to the interface. A grounded WM layer with an embedded dipole source is depicted in Fig. 15(b). The waves produced by this dipole in a WM are TM-polarized with respect to the wires, because the source dipole moment is vertical, and the magnetic vectors of the source field are parallel to xy plane.

Leaky waves created by this dipole at frequencies nearly equal to ω_p propagate from it in all azimuthal directions, with the phase velocity slightly lower than c. This is the so-called *proper leaky wave*, which is basically evanescent: it slightly decays with distance along the z axis. The real part of its tangential complex wave number $q_{\|} = k_{\|}$ is slightly larger than k.

On the contrary, leaky waves excited by a dipole at $\omega \gg \omega_p$ (but still at frequencies where the WM is effectively continuous, i.e., $\lambda > 2a$) propagate along the interface with the phase velocity much higher than c, as a fundamental mode of a hollow metal waveguide. This wave originates due to the ENZ effect, since the refractive index of our WM in this range is small ($n \ll 1$). As a result, the real part of the complex wave number in the azimuthal directions is smaller than the wavenumber k in

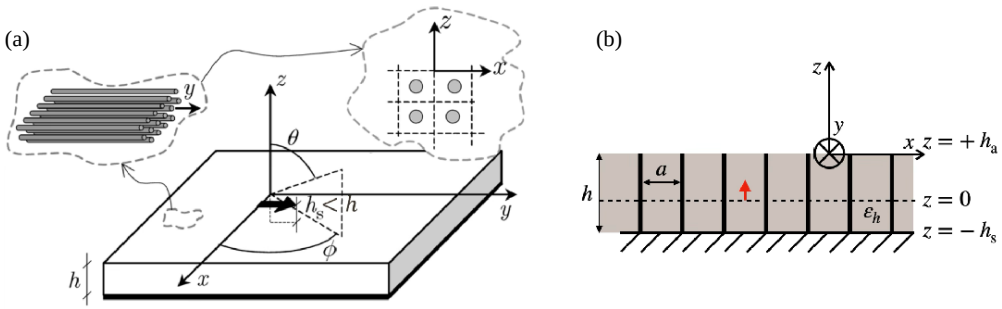

FIGURE 15. Axial dipole radiating at $\omega > \omega_p$ in a metal-backed wire medium layer. (a) Wire medium with tangentially oriented wires. (b) Wire medium with normally oriented wires. Figures are taken from [175, 176], both with the permission of publishers.

free space. The electromagnetic field amplitudes exponentially grow with z, and the wave seems to be non-physical; however, it is not so. This wave has conical wave fronts. The axis of all these cones is parallel to z and coincides with the direction of the source dipole moment. This conical wave propagates in free space obliquely to z. Across the wave front (i.e., along the wave vector), its amplitude does not grow and does not decay, because the vertical growth is compensated by the azimuthal decay. This azimuthal decay is the same inside the WM slab $\mathrm{Im}(k_\parallel) = \mathrm{Im}(q_\parallel)$, from which the energy of the corresponding slab mode leaks into free space.

In the case shown in Fig. 15(a), ABCs are not needed on the WM interfaces, and in the analytical part of [175], the issue of ABCs was not mentioned. In [176], ABCs play the key role on the top interface. Without adding them into the analytical model, the excitation of improper leaky waves could not be explained. Note that the concept of an improper leaky wave supported by a WM slab was introduced in [145], discussed above in Subsection 4.3.

5.4. Epsilon Near Zero: Interaction with Axions

In the commonly adopted theory of dark matter by Wilczek, dark-matter particles called axions interact (though very weakly) with photons. Axions in the space-time may be described by a curl-free scalar field $\alpha(\mathbf{r}, t)$. Beyond quantum electrodynamics, the interaction of this field with the electromagnetic one can be described via additional terms in two Maxwell's equations (see, e.g., [177, 178]):

$$\nabla \cdot \mathbf{D} = -g_{\alpha p} \nabla\alpha \cdot \mathbf{B}. \tag{38}$$

$$\nabla \times \mathbf{H} = \frac{\partial \mathbf{D}}{\partial t} + g_{\alpha p} \left(\frac{\partial \alpha}{\partial t} \mathbf{B} + \nabla\alpha \times \mathbf{E} \right). \tag{39}$$

Here, $g_{\alpha p}$ is the coefficient of the axion-photon interaction. Due to the smallness of this coefficient (10^{-19} 1/eV), the impact of axion terms in (38), (39) was initially considered non-measurable. The hope to detect axions was weak and associated solely with quantum effects (see, e.g., [179, 180]). In 1983, in [181], Sikivie explained that axions can be measured via the classical electromagnetic fields excited by them in classical resonators. In an ultra-high constant magnetic field $\mathbf{B}_0$, the time-varying term $g_{\alpha p}\mathbf{B}_0 \partial\alpha/\partial t$ is an effective displacement current, which can excite a resonant electromagnetic oscillation in a cavity. To obtain its amplitude sufficient for electromagnetic measurement, the axion and electromagnetic oscillation should be synchronized, and the quality factor of the resonator mode must be very high.

There are several directions in the search of axions based on the Sikivie's idea: superconducting radio-frequency cavities, microwave and THz cavities, optical cavities, and others. The corresponding works prior to 2010 can be found in the review [182]. Later works are cited in [183, 184]. Ref. [183] showed that at room temperatures, the axion field α can oscillate in the range 16 ± 1.5 GHz. More generally, the microwave range is suitable for the detection of axions in laboratory even without cryogenic cooling [150, 153, 154].

At frequencies above 10 GHz, the fundamental resonance $d = \lambda/2$ of an empty PEC cavity corresponds to its cross-section size $d < 1.5$ cm. Then, the volume in which the axion field interacts with the electromagnetic field is of the order of 3 cm^3 or smaller. Such a volume is not sufficient to produce a reliably measured amount of microwave energy.

In a larger resonator ($d \gg 1$ cm), the recommended frequency band corresponds to higher-order modes, whose quality factors are too low even in the case of precise fabrication and fine polishing of copper walls. Therefore, Ref. [185] proposed filling a copper cavity with a simple WM operating in the ENZ regime ($n \equiv \sqrt{\varepsilon_{zz}} \ll 1$). Then, the standing wave forming the cavity mode will be elongated $1/n$ times, and the cross-section of the cavity filled with the array of thin copper wires will be enlarged as $d \times d = \lambda/2n \times \lambda/2n$. Such a resonator is illustrated in Fig. 14(a). In this case, $d = 10$ cm corresponds to the 11-fold increase of the cross-section.

An accurate analytical model of this resonator takes into account the spatial dispersion of WM filling the cavity and the losses in the wires. Both these effects could critically modify the resonance mode, reducing its quality factor and disabling the idea of [185]. The resonator shown in Fig. 14(a) was studied theoretically, numerically, and experimentally in [150]. It revealed that the unloaded quality factor Q_{110} of the fundamental (TM_{110}) mode for a cubic copper cavity with an edge length of $d = 10$ cm is mainly determined by the losses in the copper WM, and the losses in the walls are negligibly small. However, Q_{110} attains the suitable value $3 \cdot 10^3$ for plasma frequencies of 15–20 GHz even at room temperatures. For lower plasma frequencies, Q_{110} increases (at 5 GHz, $Q_{110} \approx 6 \cdot 10^3$). However, the experimental value of loaded quality factor Q_l is signifi-

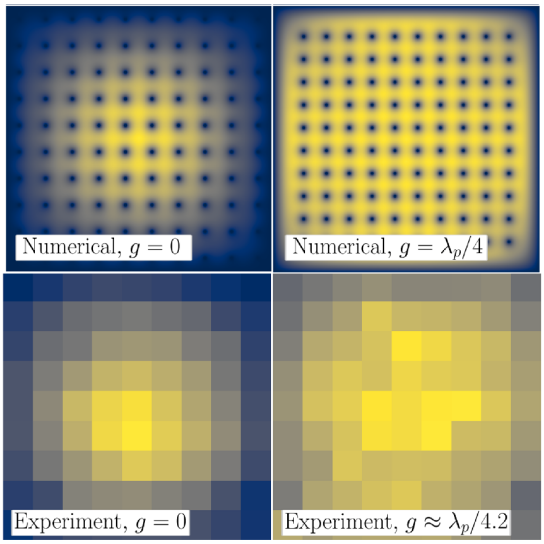

FIGURE 16. Distribution of the electric field intensity (z-component in the xy plane) in the WM cavity created for the axion search of conventional ($d = \lambda_p/2n$) and enlarged ($d = \lambda_p/2n + 2g$) sizes. Figures are taken from [155] with the permission of publishers.

cantly lower. For a well-prepared realistic probe, [150] theoretically predicted $Q_l \approx Q_{110}/2$, which is confirmed by their measurement. In general, the experimental results of this work are in good agreement with the theory (which, in turn, is in excellent agreement with full-wave simulations). Note that in the experimental sample studied in [150], the WM had the plasma frequency 11.45 GHz.

The next step in this direction was to create a WM-filled resonator with tunable plasma frequency. For this purpose, [82] used a nested simple WM concept. By shifting one array of parallel wires with respect to the other one by vector $\mathbf{\Delta}$, as shown in Fig. 4(b), the authors found the plasma frequencies for different values of $\mathbf{\Delta}$. The evident drawback of this technical solution was the necessity to build the resonators for all experimental values of $\mathbf{\Delta}$. Ref. [186] achieved tunability with a different solution — wires of oblong cross section, not soldered to the top and bottom walls, but passing through them, ended with usual screws.

The concept of thin wires allows the radii of the cross-section to be equal to $r_0 = 0.1a$. If we replace such wires by strips of width $w = 4r_0$ (see above), this width is $w = 0.4a$, i.e., comparable with the WM period. If these substantially wide strips are oriented parallel to the x (or y) axis, the WM with a square unit cell ($a = b$) becomes noticeably anisotropic in the xy plane [186]. By rotating different sets of wires in different ways, we can restore the in-plane isotropy of our WM, transforming it into a nested WM. However, metal strips (oblong rectangles) possess high electromagnetic losses due to the edges. Therefore, if we employ usual copper strips as wires, the needed Q-factor cannot be achieved even at the fundamental resonance. To restore the high quality factor, in [186], the corners of the rectangular cross-section of a constitutive strip were rounded, and the corresponding WM was called an *obround nested WM*. By simply adjusting the screws, ω_p tunability of about 30% was achieved without compromising the quality factor compared to usual wires studied by the same team in [150]. An even better tunability of ω_p (more than 50%) was achieved in [187] using breathing mechanical deformations of a simple WM (with a honeycomb lattice of usual wires). However, the implementation of this technical solution is more difficult.

This structure (called the *microwave plasma haloscope*) was further advanced in 155]. To enhance the effective volume in which the axion field interacts with the electromagnetic one, the cavity cross-section was enlarged so that the lateral cavity walls were located at the distance $g \approx \lambda/4$ from the WM sample. Since in the operation band $\lambda \approx \lambda_p$, this condition can be written as $g \approx \lambda_p/4$. In a simplistic insight, when $g = \lambda/4$, the WM sample is effectively bounded by magnetic walls. In the gaps between these virtual walls and the real walls of the cavity, the z-polarized electric field decreases in accordance to the cosine law, but across the WM sample, theoretically, it should be uniform. Replacing the cosine distribution of the electric field by the uniform distribution effectively increases the mode volume. Therefore, the electromagnetic energy generated by axions should be enhanced. Numerical and experimental studies confirmed the field uniformity across the WM sample for the enlarged cavity. In Fig. 16, the numerically simulated (top panel) and measured (bottom panel) electric intensity distributions in the xy plane are shown for both $g = 0$ and $g \approx \lambda_p/4$. Experiment showed that the optimal gap for the used copper cavity was $\lambda_p/4.2$ (that difference could result from metal impurities). The granularity of the experimental intensity map is determined by the discreteness of the probe positions (centers of the WM unit cells).

5.5. Super-Emission and Super-Absorbance

Several years before the publication of [172], Ref. [188] theoretically found that a WM layer operating in the mid-infrared range combined with a thermal emitter, with the wires partially embedded into the heated medium, drastically enhances the thermal emission of atoms located between the nanowires. Using the terminology of [172], this enhancement can be explained by the Purcell effect, which is very strong at frequencies lower than the plasma frequency of the WM. Only one third of atoms is polarized along the z axis; two thirds of them are polarized perpendicular to the wires; and their thermal radiation in absence of the nanowires, described by the Planck law, is multiplied by the Purcell factor, which is very high. This radiation is called *super-Planckian*. It propagates along the nanowires, but is locked on the top interface of the WM and exponentially decays away from it. This super-Planckian near-field thermal emission can be used for the enhancement of the so-called *thermophotovoltaic generators of electricity* [19, 188].

In [3, 189] published in 2007, an object located at the narrow end of a tapered (conical) WM endoscope created a TM-polarized wave packet carrying its subwavelength image. In the form of a packet of non-uniform TEM waves, this image was canalized along the wires towards the base of the cone and radiated from it to free space. In the far zone, this radiation resulted in a magnified far-field subwavelength image of the object.

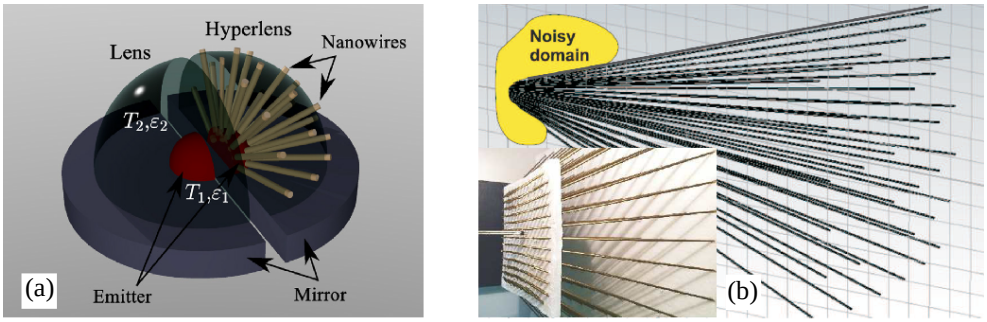

FIGURE 17. Super-emitter obtained with a WM hyperlens. (a) Super-Planckian thermal emission. (b) Super-emission from the noisy region. Figures are taken from [20, 165], both with the permission of publishers.

A similar enhancement mechanism is involved in super-Planckian thermal emission, which was theoretically and numerically shown in [20]. The suggested thermal super-emitter is schematically depicted in Fig. 17(a). The super-Planckian emission is canalized towards the wide end of the hemispherical sample of radially divergent nanowires. Due to WM tapering, the surface impedance on its top interface becomes close to that of free space in the entire band of the thermal radiation. Therefore, the super-Planckian emission is radiated to the far zone of the structure. Ref. [20] called this structure a *wire-medium hyperlens*.

We have discussed this infrared study, because similar physics underlies the operation of tapered microwave WM, where microwave noise plays the role of thermal emission. When the wires touch a noisy region, the Purcell effect enhances this noise, with the TM-polarized part canalized towards the broad end of the endoscope and radiated from this end. Via the known Purcell factor of the WM in the narrow part of the endoscope, the spectroscopic measurements of the noise in the far zone allow retrieving the original noise spectrum. For microwave noise created by nanoelectronic devices, the WM hyperlens suggested in [165] can replace conventional near-field probes, which cannot operate without amplifiers, creating their own noise [190].

In [165], a microwave WM hyperlens was studied analytically, numerically, and experimentally. In Fig. 17(b), the schematic and the photo of the experimental sample are shown. The results of [165] were further developed in [10].

Super-emission is a linear reciprocal effect, and it also implies super-absorbance. If a wave falls on the broad end of a WM hyperlens (of conical shape with an absorber at the apex, or of spherical shape with an absorber in the center), its energy is captured by the array of radially divergent wires and canalized towards the absorber. The absorption cross-section of this structure strongly exceeds that of an individual absorber in free space. It is nearly equal to the maximal cross-section of the WM hyperlens (the base of a WM cone or the cross-section of a WM sphere). Ref. [21] showed that the absorption cross-section of a spherical metamaterial hyperlens with an absorber in the center can be even larger than its physical cross-section. However, this effect cannot be achieved using only a WM. For this additional enhancement of the absorbance, a more sophisticated (and non-homogeneous) metamaterial is needed [21].

6. CONCLUSION

The first purpose of the present review was to introduce the readers to reliable theoretical models of microwave wire media — validated experimentally or at least by sufficiently extensive full-wave simulations. Our second purpose will be explained below.

Wire media stand out among other metamaterials due to their strong spatial dispersion. This phenomenon is rarely inherent to effectively continuous media called materials, whose electromagnetic response can be described by effective material parameters, such as the permittivity dyadic. Unlike dielectric, metallic, or semiconductor photonic crystals, for which we can also introduce the effective permittivity dependent on the wave vector $\mathbf{q}$, relevant only for the eigenmode dispersion analysis, WM are described by an effective permittivity that remains valid in the solution of boundary problems. Its $\mathbf{q}$-dependence results not from electromagnetically large periods of the lattice (unlike photonic crystals, the periods of WM lattices are by definition much smaller than the wavelength in the host medium), but from far-field interactions of the wires. This wave interaction proves to be more significant than the quasi-static (near-field) one.

We have reviewed theoretical models of unbounded WM of different types, which allowed deriving the spatially dispersive effective permittivity tensors in the explicit form and analyzing the eigenmode dispersion. We presented the main boundary problems with microwave WM and reviewed the most important physical effects observed in them. Above, we noted the great potential for future WM research. Let us better emphasize this point. Further investigations of WM are highly promising due to two factors: (1) the existing theory of WM is severely underdeveloped, and (2) the already revealed physical effects in WM leave no doubt that a great variety of physical effects in WM (and their potential applications) will be revealed in future.

Recall that the history of simple WM counts 80 years. However, such an essential phenomenon as radiation of internal sources, and such key characteristics of the eigenmodes as power flux and energy density have been studied only quite recently, and only for the special case — a rectangular lattice of parallel wires having the same cross-section. Even for simple WM of different geometries — nested WM or WM with a triangular unit cell — these key issues have been never studied, to

our knowledge. Known theories of other types of WM do not even mention these issues. Specific WM models are usually limited to the analysis of the eigenmode dispersion and polarization. Additional boundary conditions, necessary for many boundary problems with WM, are established not for all types of WM and not for all possible wire terminations.

We discussed and cited a large number of papers dedicated to WM; however, this body of literature is an evidence of the great potential of WM research and not of their deep exploration. If this review motivates some readers to delve into the unexplored areas of this field, the authors will achieve their second purpose.

ACKNOWLEDGEMENT

Authors thank Lydia Pogorelskaya for proofreading.

REFERENCES

[1] Simovski, C. R., P. A. Belov, A. V. Atrashchenko, and Y. S. Kivshar, "Wire metamaterials: Physics and applications," *Advanced Materials*, Vol. 24, No. 31, 4229–4248, 2012.

[2] Ikonen, P., C. Simovski, and S. Tretyakov, "Compact directive antennas with a wire-medium artificial lens," *Microwave and Optical Technology Letters*, Vol. 43, No. 6, 467–469, 2004.

[3] Ikonen, P., C. Simovski, S. Tretyakov, P. Belov, and Y. Hao, "Magnification of subwavelength field distributions at microwave frequencies using a wire medium slab operating in the canalization regime," *Applied Physics Letters*, Vol. 91, No. 10, 104102, 2007.

[4] Tuniz, A., K. J. Kaltenecker, B. M. Fischer, M. Walther, S. C. Fleming, A. Argyros, and B. T. Kuhlmey, "Metamaterial fibres for subdiffraction imaging and focusing at terahertz frequencies over optically long distances," *Nature Communications*, Vol. 4, No. 1, 2706, 2013.

[5] Ono, A., J.-I. Kato, and S. Kawata, "Subwavelength optical imaging through a metallic nanorod array," *Physical Review Letters*, Vol. 95, No. 26, 267407, 2005.

[6] Nordlander, P., "Subwavelength imaging in colour," *Nature Photonics*, Vol. 2, No. 7, 387–388, 2008.

[7] Lerosey, G., J. de Rosny, A. Tourin, and M. Fink, "Focusing beyond the diffraction limit with far-field time reversal," *Science*, Vol. 315, No. 5815, 1120–1122, 2007.

[8] Lemoult, F., G. Lerosey, J. de Rosny, and M. Fink, "Resonant metalenses for breaking the diffraction barrier," *Physical Review Letters*, Vol. 104, No. 20, 203901, 2010.

[9] Lemoult, F., M. Fink, and G. Lerosey, "Revisiting the wire medium: An ideal resonant metalens," *Waves in Random and Complex Media*, Vol. 21, No. 4, 591–613, 2011.

[10] Kosulnikov, S. Y., M. S. Mirmoosa, D. A. Vovchuk, S. A. Tretyakov, S. B. Glybovski, and C. R. Simovski, "Enhancement of radiation with irregular wire media," *IEEE Transactions on Antennas and Propagation*, Vol. 64, No. 12, 5469–5474, 2016.

[11] Caloz, C. and T. Itoh, *Electromagnetic Metamaterials: Transmission Line Theory and Microwave Applications*, John Wiley & Sons, 2005.

[12] Eleftheriades, G. V. and K. G. Balmain, *Negative-Refraction Metamaterials: Fundamental Principles and Applications*, John Wiley & Sons, 2005.

[13] Engheta, N. and R. W. Ziolkowski, *Electromagnetic Metamaterials: Physics and Engineering Explorations*, IEEE Press, Piscataway, NJ, 2006.

[14] Capolino, F., *Metamaterials Handbook. Vol. 1: Theory and Phenomena of Metamaterials*, CRC Press, Boca Raton, CA, 2009.

[15] Capolino, F., *Metamaterials Handbook. Vol. 2: Applications of Metamaterials*, CRC Press, Boca Raton, CA, 2009.

[16] Cai, W. and V. Shalaev, *Optical Metamaterials: Fundamentals and Applications*, Springer, 2010.

[17] Radu, X., D. Garray, and C. Craeye, "Toward a wire medium endoscope for MRI imaging," *Metamaterials*, Vol. 3, No. 2, 90–99, 2009.

[18] Slobozhanyuk, A. P., I. V. Melchakova, A. V. Kozachenko, D. S. Filonov, C. R. Simovski, and P. A. Belov, "An endoscope based on extremely anisotropic metamaterials for applications in magnetic resonance imaging," *Journal of Communications Technology and Electronics*, Vol. 59, No. 6, 562–570, 2014.

[19] Mirmoosa, M. S. and C. Simovski, "Micron-gap thermophotovoltaic systems enhanced by nanowires," *Photonics and Nanostructures — Fundamentals and Applications*, Vol. 13, 20–30, 2015.

[20] Simovski, C., S. Maslovski, I. Nefedov, S. Kosulnikov, P. Belov, and S. Tretyakov, "Hyperlens makes thermal emission strongly super-Planckian," *Photonics and Nanostructures — Fundamentals and Applications*, Vol. 13, 31–41, 2015.

[21] Maslovski, S. I., C. R. Simovski, and S. A. Tretyakov, "Overcoming black body radiation limit in free space: Metamaterial superemitter," *New Journal of Physics*, Vol. 18, No. 1, 013034, 2016.

[22] Kawata, S., A. Ono, and P. Verma, "Subwavelength colour imaging with a metallic nanolens," *Nature Photonics*, Vol. 2, No. 7, 438–442, 2008.

[23] Casse, B. D. F., W. T. Lu, Y. J. Huang, E. Gultepe, L. Menon, and S. Sridhar, "Super-resolution imaging using a three-dimensional metamaterials nanolens," *Applied Physics Letters*, Vol. 96, No. 2, 023114, 2010.

[24] Liu, Y., G. Bartal, and X. Zhang, "All-angle negative refraction and imaging in a bulk medium made of metallic nanowires in the visible region," *Optics Express*, Vol. 16, No. 20, 15 439–15 448, 2008.

[25] Landau, L. D. and E. M. Lifshitz, *Electrodynamics of Continuous Media*, 2nd ed., Pergamon, New York, 1984.

[26] Lu, Z. and D. W. Prather, "Calculation of effective permittivity, permeability, and surface impedance of negative-refraction photonic crystals," *Optics Express*, Vol. 15, No. 13, 8340–8345, 2007.

[27] Brekhovskikh, L., *Waves in Layered Media*, Academic Press, New York, 1980.

[28] Sievenpiper, D., L. Zhang, R. F. J. Broas, N. G. Alexopolous, and E. Yablonovitch, "High-impedance electromagnetic surfaces with a forbidden frequency band," *IEEE Transactions on Microwave Theory and Techniques*, Vol. 47, No. 11, 2059–2074, 1999.

[29] Tretyakov, S., *Analytical Modeling in Applied Electromagnetics*, Artech House, 2003.

[30] Luukkonen, O., C. R. Simovski, and S. Tretyakov, "Grounded uniaxial material slabs as magnetic conductors," *Progress In Electromagnetics Research B*, Vol. 15, 267–283, 2009.

[31] Maslovski, S. I., T. A. Morgado, M. G. Silveirinha, C. S. R. Kaipa, and A. B. Yakovlev, "Generalized additional boundary conditions for wire media," *New Journal of Physics*, Vol. 12, No. 11, 113047, 2010.

[32] Hanson, G. W., M. G. Silveirinha, P. Burghignoli, and A. B. Yakovlev, "Non-local susceptibility of the wire medium in the spatial domain considering material boundaries," *New Journal*

of Physics, Vol. 15, No. 8, 083018, 2013.

[33] Lannebère, S., T. A. Morgado, and M. G. Silveirinha, "First principles homogenization of periodic metamaterials and application to wire media," *Comptes Rendus. Physique*, Vol. 21, No. 4–5, 367–388, 2020.

[34] Von Ignatowsky, W., "Zur theorie der gitter," *Annalen der Physik*, Vol. 349, No. 11, 369–436, 1914.

[35] MacFarlane, G. G., "Surface impedance of an infinite parallel-wire grid at oblique angles of incidence," *Journal of the Institution of Electrical Engineers — Part IIIA: Radiolocation*, Vol. 93, No. 10, 1523–1527, 1946.

[36] Lewis, E. A. and J. P. Casey Jr., "Electromagnetic reflection and transmission by gratings of resistive wires," *Journal of Applied Physics*, Vol. 23, No. 6, 605–608, 1952.

[37] Decker, M. T., "Transmission and reflection by a parallel wire grid," *Journal of Research of the National Bureau of Standards, Section D: Radio Propagation*, Vol. 63, No. 1, 87–90, 1959.

[38] Kock, W. E., "Metal-lens antennas," *Proceedings of the IRE*, Vol. 34, No. 11, 828–836, 1946.

[39] Kock, W. E., "Metallic delay lenses," *Bell System Technical Journal*, Vol. 27, No. 1, 58–82, 1948.

[40] Brown, J., "Artificial dielectrics having refractive indices less than unity," *Proceedings of the IEE — Part IV: Institution Monographs*, Vol. 100, No. 5, 51–62, 1953.

[41] Brown, J., "Artificial dielectrics," *Progress in Dielectrics*, Vol. 2, 195–225, J. B. Birks and J. H. Schulman (eds.), Heywood & Company Ltd., London, 1960.

[42] Rotman, W., "Plasma simulation by artificial dielectrics and parallel-plate media," *IRE Transactions on Antennas and Propagation*, Vol. 10, No. 1, 82–95, 1962.

[43] Carne, A. and J. Brown, "Theory of reflections from the rodded-type artificial dielectric," *Proceedings of the IEE — Part B: Radio and Electronic Engineering*, Vol. 106, No. 26, 107–114, 1959.

[44] Pendry, J. B., A. J. Holden, W. J. Stewart, and I. Youngs, "Extremely low frequency plasmons in metallic mesostructures," *Physical Review Letters*, Vol. 76, No. 25, 4773, Jun. 1996.

[45] Pendry, J. B., A. J. Holden, D. J. Robbins, and W. J. Stewart, "Low frequency plasmons in thin-wire structures," *Journal of Physics: Condensed Matter*, Vol. 10, No. 22, 4785, 1998.

[46] Belov, P. A., S. A. Tretyakov, and A. J. Viitanen, "Dispersion and reflection properties of artificial media formed by regular lattices of ideally conducting wires," *Journal of Electromagnetic Waves and Applications*, Vol. 16, No. 8, 1153–1170, 2002.

[47] Belov, P. A., C. R. Simovski, and S. A. Tretyakov, "Two-dimensional electromagnetic crystals formed by reactively loaded wires," *Physical Review E*, Vol. 66, No. 3, 036610, 2002.

[48] Belov, P. A., R. Marqués, S. I. Maslovski, I. S. Nefedov, M. Silveirinha, C. R. Simovski, and S. A. Tretyakov, "Strong spatial dispersion in wire media in the very large wavelength limit," *Physical Review B*, Vol. 67, No. 11, 113103, 2003.

[49] Simovski, C. R. and P. A. Belov, "Low-frequency spatial dispersion in wire media," *Physical Review E*, Vol. 70, No. 4, 046616, 2004.

[50] Silveirinha, M. G. and C. A. Fernandes, "Homogenization of 3-D-connected and nonconnected wire metamaterials," *IEEE Transactions on Microwave Theory and Techniques*, Vol. 53, No. 4, 1418–1430, 2005.

[51] Silveirinha, M. G., "Nonlocal homogenization model for a periodic array of epsilon-negative rods," *Physical Review E*, Vol. 73, No. 4, 046612, 2006.

[52] Maslovski, S. I., S. A. Tretyakov, and P. A. Belov, "Wire media with negative effective permittivity: A quasi-static model," *Microwave and Optical Technology Letters*, Vol. 35, No. 1, 47–51, 2002.

[53] Tyukhtin, A. V. and E. G. Doilnitsina, "Effective permittivity of a metamaterial from coated wires," *Journal of Physics D: Applied Physics*, Vol. 44, No. 26, 265401, 2011.

[54] Sakhno, D., R. Balafendiev, and P. A. Belov, "Anisotropy in a wire medium resulting from the rectangularity of a unit cell," *Physical Review B*, Vol. 110, No. 14, L140303, 2024.

[55] Nicorovici, N. A., R. C. McPhedran, and L. C. Botten, "Photonic band gaps for arrays of perfectly conducting cylinders," *Physical Review E*, Vol. 52, No. 1, 1135, 1995.

[56] Smirnova, E. I., C. Chen, M. A. Shapiro, J. R. Sirigiri, and R. J. Temkin, "Simulation of photonic band gaps in metal rod lattices for microwave applications," *Journal of Applied Physics*, Vol. 91, No. 3, 960–968, 2002.

[57] Silveirinha, M. G. and C. A. Fernandes, "Efficient calculation of the band structure of artificial materials with cylindrical metallic inclusions," *IEEE Transactions on Microwave Theory and Techniques*, Vol. 51, No. 5, 1460–1466, 2003.

[58] Cohn, S. B., "Analysis of the metal-strip delay structure for microwave lenses," *Journal of Applied Physics*, Vol. 20, No. 3, 257–262, 1949.

[59] Brown, J., "The design of metallic delay dielectrics," *Proceedings of the IEE — Part III: Radio and Communication Engineering*, Vol. 97, No. 45, 45–48, 1950.

[60] Veselago, V. G., "The electrodynamics of substances with simultaneously negative values of ϵ and μ," *Soviet Physics Uspekhi*, Vol. 10, 509–514, 1968.

[61] Pendry, J. B., "Negative refraction makes a perfect lens," *Physical Review Letters*, Vol. 85, No. 18, 3966, 2000.

[62] Smith, D. R., D. C. Vier, N. Kroll, and S. Schultz, "Direct calculation of permeability and permittivity for a left-handed metamaterial," *Applied Physics Letters*, Vol. 77, No. 14, 2246–2248, 2000.

[63] Shelby, R. A., D. R. Smith, and S. Schultz, "Experimental verification of a negative index of refraction," *Science*, Vol. 292, No. 5514, 77–79, 2001.

[64] Simovski, C. R. and B. Sauviac, "Toward creating isotropic microwave composites with negative refraction," *Radio Science*, Vol. 39, No. 2, 1–18, 2004.

[65] Verney, E., B. Sauviac, and C. R. Simovski, "Isotropic metamaterial electromagnetic lens," *Physics Letters A*, Vol. 331, No. 3–4, 244–247, 2004.

[66] Silveirinha, M. G., P. A. Belov, and C. R. Simovski, "Ultimate limit of resolution of subwavelength imaging devices formed by metallic rods," *Optics Letters*, Vol. 33, No. 15, 1726–1728, 2008.

[67] Sarychev, A. K. and V. M. Shalaev, "Comment on paper 'Extremely low frequency plasmons in metallic mesostructures'," *arXiv:cond-mat/0103145*, 2001.

[68] Shvets, G., A. K. Sarychev, and V. M. Shalaev, "Electromagnetic properties of three-dimensional wire arrays: Photons, plasmons, and equivalent circuits," in *Complex Mediums IV: Beyond Linear Isotropic Dielectrics*, Vol. 5218, 156–165, 2003.

[69] Maslovski, S. I. and M. G. Silveirinha, "Non-local permittivity from a quasi-static model for a class of wire media," *Physical Review B*, Vol. 80, No. 24, 245101, 2009.

[70] Kumar, A., A. Majumder, S. Chatterjee, S. Das, and S. Kar, "A novel approach to determine the plasma frequency for wire media," *Metamaterials*, Vol. 6, No. 1–2, 43–50, 2012.

[71] Sakhno, D. and P. A. Belov, "Plasma frequency of wire medium revisited," *arXiv preprint arXiv:2505.17900*, 2025.

[72] Brand, S., R. A. Abram, and M. A. Kaliteevski, "Complex photonic band structure and effective plasma frequency of a two-dimensional array of metal rods," *Physical Review B*, Vol. 75, No. 3, 035102, 2007.

[73] Agranovich, V. M. and V. Ginzburg, *Crystal Optics with Spatial Dispersion, and Excitons*, Springer Science & Business Media, 2013.

[74] Krall, N. A. and A. W. Trivelpiece, *Principles of Plasma Physics*, McGraw-Hill, 1973.

[75] Pokrovsky, A. L. and A. L. Efros, "Electrodynamics of metallic photonic crystals and the problem of left-handed materials," *Physical Review Letters*, Vol. 89, No. 9, 093901, 2002.

[76] Tretyakov, S. A., I. S. Nefedov, C. R. Simovski, and S. I. Maslovski, "Modelling and microwave properties of artificial materials with negative parameters," in *Advances in Electromagnetics of Complex Media and Metamaterials*, 99–122, Springer Science & Business Media, 2002.

[77] Simovski, C. R., P. A. Belov, and S. He, "Backward wave region and negative material parameters of a structure formed by lattices of wires and split-ring resonators," *IEEE Transactions on Antennas and Propagation*, Vol. 51, No. 10, 2582–2591, 2003.

[78] Pokrovsky, A. L. and A. L. Efros, "Nonlocal electrodynamics of two-dimensional wire mesh photonic crystals," *Physical Review B*, Vol. 65, No. 4, 045110, 2002.

[79] Pokrovsky, A. L., "Analytical and numerical studies of wire-mesh metallic photonic crystals," *Physical Review B*, Vol. 69, No. 19, 195108, 2004.

[80] Gorlach, M. A., M. Song, A. P. Slobozhanyuk, A. A. Bogdanov, and P. A. Belov, "Topological transition in coated wire medium," *Physica Status Solidi (RRL) — Rapid Research Letters*, Vol. 10, No. 12, 900–904, 2016.

[81] Fernandes, D. E., S. I. Maslovski, G. W. Hanson, and M. G. Silveirinha, "Fano resonances in nested wire media," *Physical Review B*, Vol. 88, No. 4, 045130, 2013.

[82] Kowitt, N., R. Balafendiev, D. Sun, M. Wooten, A. Droster, M. A. Gorlach, K. Van Bibber, and P. A. Belov, "Tunable wire metamaterials for an axion haloscope," *Physical Review Applied*, Vol. 20, No. 4, 044051, 2023.

[83] Agranovich, V. M. and V. L. Ginzburg, *Spatial Dispersion in Crystal Optics and the Theory of Excitons*, Wiley, 1966.

[84] Silveirinha, M. G. and S. I. Maslovski, "Radiation from elementary sources in a uniaxial wire medium," *Physical Review B*, Vol. 85, No. 15, 155125, 2012.

[85] Koreshin, E. A., D. Sakhno, J. A. Enriquez, and P. A. Belov, "Single-shot near-field reconstruction of metamaterial dispersion," *Physical Review B*, Vol. 113, No. 10, 104302, 2026.

[86] Nefedov, I. S., A. J. Viitanen, and S. A. Tretyakov, "Electromagnetic wave refraction at an interface of a double wire medium," *Physical Review B*, Vol. 72, No. 24, 245113, 2005.

[87] Nefedov, I. S., A. J. Viitanen, and S. A. Tretyakov, "Propagating and evanescent modes in two-dimensional wire media," *Physical Review E*, Vol. 71, No. 4, 046612, 2005.

[88] Silveirinha, M. G. and C. A. Fernandes, "Nonresonant structured material with extreme effective parameters," *Physical Review B*, Vol. 78, No. 3, 033108, 2008.

[89] Silveirinha, M. G., C. A. Fernandes, and J. R. Costa, "Superlens made of a metamaterial with extreme effective parameters," *Physical Review B*, Vol. 78, No. 19, 195121, 2008.

[90] Silveirinha, M. G., "Anomalous refraction of light colors by a metamaterial prism," *Physical Review Letters*, Vol. 102, No. 19, 193903, 2009.

[91] Poddubny, A., I. Iorsh, P. Belov, and Y. Kivshar, "Hyperbolic metamaterials," *Nature Photonics*, Vol. 7, No. 12, 948–957, 2013.

[92] Sakhno, D., E. Koreshin, and P. Belov, "Quadraxial metamaterial," *Optics Letters*, Vol. 47, No. 17, 4451–4454, 2022.

[93] Morgado, T. A., J. S. Marcos, J. T. Costa, J. R. Costa, C. A. Fernandes, and M. G. Silveirinha, "Reversed rainbow with a nonlocal metamaterial," *Applied Physics Letters*, Vol. 105, No. 26, 264101, 2014.

[94] Salakhova, N. S., I. M. Fradkin, S. A. Dyakov, and N. A. Gippius, "Fourier modal method for moiré lattices," *Physical Review B*, Vol. 104, No. 8, 085424, 2021.

[95] Hu, G., A. Krasnok, Y. Mazor, C.-W. Qiu, and A. Alù, "Moiré hyperbolic metasurfaces," *Nano Letters*, Vol. 20, No. 5, 3217–3224, 2020.

[96] Salakhova, N. S., I. M. Fradkin, S. A. Dyakov, and N. A. Gippius, "Twist-tunable moiré optical resonances," *Physical Review B*, Vol. 107, No. 15, 155402, 2023.

[97] Chang, A. S. P., Y. S. Kim, M. Chen, Z.-P. Yang, J. A. Bur, S.-Y. Lin, and K.-M. Ho, "Visible three-dimensional metallic photonic crystal with non-localized propagating modes beyond waveguide cutoff," *Optics Express*, Vol. 15, No. 13, 8428–8437, 2007.

[98] Silveirinha, M. G. and C. A. Fernandes, "A hybrid method for the efficient calculation of the band structure of 3-D metallic crystals," *IEEE Transactions on Microwave Theory and Techniques*, Vol. 52, No. 3, 889–902, 2004.

[99] Born, M. and E. Wolf, *Principles of Optics: Electromagnetic Theory of Propagation, Interference and Diffraction of Light*, Elsevier, 2013.

[100] Turpin, A., Y. V. Loiko, T. K. Kalkandjiev, and J. Mompart, "Conical refraction: Fundamentals and applications," *Laser & Photonics Reviews*, Vol. 10, No. 5, 750–771, 2016.

[101] Sözüer, H. S. and J. W. Haus, "Photonic bands: Simple-cubic lattice," *Journal of the Optical Society of America B*, Vol. 10, No. 2, 296–302, 1993.

[102] Sigalas, M. M., C. T. Chan, K. M. Ho, and C. M. Soukoulis, "Metallic photonic band-gap materials," *Physical Review B*, Vol. 52, No. 16, 11744, 1995.

[103] Sievenpiper, D. F., M. E. Sickmiller, and E. Yablonovitch, "3D wire mesh photonic crystals," *Physical Review Letters*, Vol. 76, No. 14, 2480, 1996.

[104] Silveirinha, M. G., "Artificial plasma formed by connected metallic wires at infrared frequencies," *Physical Review B*, Vol. 79, No. 3, 035118, 2009.

[105] Hudlicka, M., J. Machac, and I. Nefedov, "A triple wire medium as an isotropic negative permittivity metamaterial," *Progress In Electromagnetics Research*, Vol. 65, 233–246, 2006.

[106] Demetriadou, A. and J. B. Pendry, "Taming spatial dispersion in wire metamaterial," *Journal of Physics: Condensed Matter*, Vol. 20, No. 29, 295222, 2008.

[107] Chen, W.-J., B. Hou, Z.-Q. Zhang, J. B. Pendry, and C. T. Chan, "Metamaterials with index ellipsoids at arbitrary k-points," *Nature Communications*, Vol. 9, No. 1, 2086, 2018.

[108] Lourtioz, J.-M. and A. de Lustrac, "Metallic photonic crystals," *Comptes Rendus Physique*, Vol. 3, No. 1, 79–88, 2002.

[109] Kafesaki, M., I. Tsiapa, N. Katsarakis, T. Koschny, C. M. Soukoulis, and E. N. Economou, "Left-handed metamaterials: The fishnet structure and its variations," *Physical Review B*, Vol. 75, No. 23, 235114, Jun. 2007.

[110] Beruete, M., M. Sorolla, and I. Campillo, "Left-handed extraordinary optical transmission through a photonic crystal of subwavelength hole arrays," *Optics Express*, Vol. 14, No. 12,

5445–5455, 2006.

[111] Mary, A., S. G. Rodrigo, F. J. Garcia-Vidal, and L. Martin-Moreno, "Theory of negative-refractive-index response of double-fishnet structures," *Physical Review Letters*, Vol. 101, No. 10, 103902, Sep. 2008.

[112] Du, Q., H. Yang, X. Wang, and T. Lv, "An improved fish-net three-dimensional metamaterial with multiband left-handed characteristics at terahertz frequencies," *Optics Communications*, Vol. 285, No. 6, 980–985, 2012.

[113] Mary, A., S. G. Rodrigo, L. Martín-Moreno, and F. J. García-Vidal, "Holey metal films: From extraordinary transmission to negative-index behavior," *Physical Review B*, Vol. 80, No. 16, 165431, Oct. 2009.

[114] Navarro-Cía, M., M. Beruete, M. Sorolla, and I. Campillo, "Negative refraction in a prism made of stacked subwavelength hole arrays," *Optics Express*, Vol. 16, No. 2, 560–566, 2008.

[115] Beruete, M., I. Campillo, M. Navarro-Cia, F. Falcone, and M. S. Ayza, "Molding left-or right-handed metamaterials by stacked cutoff metallic hole arrays," *IEEE Transactions on Antennas and Propagation*, Vol. 55, No. 6, 1514–1521, 2007.

[116] Shin, J., J.-T. Shen, and S. Fan, "Three-dimensional electromagnetic metamaterials that homogenize to uniform non-Maxwellian media," *Physical Review B*, Vol. 76, No. 11, 113101, 2007.

[117] Latioui, H. and M. G. Silveirinha, "Light tunneling anomaly in interlaced metallic wire meshes," *Physical Review B*, Vol. 96, No. 19, 195132, 2017.

[118] Powell, A. W., R. C. Mitchell-Thomas, S. Zhang, D. A. Cadman, A. P. Hibbins, and J. R. Sambles, "Dark mode excitation in three-dimensional interlaced metallic meshes," *ACS Photonics*, Vol. 8, No. 3, 841–846, 2021.

[119] Sakhno, D., E. Koreshin, and P. A. Belov, "Longitudinal electromagnetic waves with extremely short wavelength," *Physical Review B*, Vol. 104, L100304, 2021.

[120] Wang, W., A. Günzler, B. D. Wilts, U. Steiner, and M. Saba, "Unconventional bound states in the continuum from metamaterial-induced electron acoustic waves," *Advanced Photonics*, Vol. 5, No. 5, 056005, 2023.

[121] Hanson, G. W., E. Forati, and M. G. Silveirinha, "Modeling of spatially-dispersive wire media: Transport representation, comparison with natural materials, and additional boundary conditions," *IEEE Transactions on Antennas and Propagation*, Vol. 60, No. 9, 4219–4232, 2012.

[122] Sakhno, D., E. Koreshin, and P. A. Belov, "Controlling the dispersion of longitudinal waves via the affine deformation of the interlaced wire medium," *Photonics and Nanostructures — Fundamentals and Applications*, Vol. 55, 101150, 2023.

[123] Liu, J.-Y., J.-W. Dong, and W.-J. Chen, "Directional emission of a three-dimensional connection-type metamaterial," *Optics Letters*, Vol. 49, No. 4, 1029–1032, 2024.

[124] De Jonghe, J. and R. Keppens, "A two-fluid analysis of waves in a warm ion-electron plasma," *Physics of Plasmas*, Vol. 27, No. 12, 122107, 2020.

[125] Pekar, S. I., "The theory of electromagnetic waves in a crystal in which excitons are produced," *Soviet Physics JETP*, Vol. 6, No. 33, 785, 1958.

[126] Kim, S., E. F. Kuester, C. L. Holloway, A. D. Scher, and J. Baker-Jarvis, "Boundary effects on the determination of metamaterial parameters from normal incidence reflection and transmission measurements," *IEEE Transactions on Antennas and Propagation*, Vol. 59, No. 6, 2226–2240, 2011.

[127] Silveirinha, M. G., "Additional boundary condition for the wire medium," *IEEE Transactions on Antennas and Propagation*, Vol. 54, No. 6, 1766–1780, 2006.

[128] Maslovski, S. I., T. A. Morgado, and M. G. Silveirinha, "The auxiliary source method and its application to the reflection problem at an interface with tilted wires," in *2010 URSI International Symposium on Electromagnetic Theory*, 319–322, Berlin, Germany, 2010.

[129] Movahediqomi, M., Y. Li, G. Ptitcyn, V. Asadchy, and S. Tretyakov, "Simultaneous perfect anomalous reflection and angle of arrival sensing in reconfigurable intelligent surfaces," *Advanced Optical Materials*, Vol. 13, No. 13, 2403033, 2025.

[130] Vuyyuru, S. K. R., M. Movahediqomi, G. Ptitcyn, R. Valkonen, V. S. Asadchy, D.-H. Kwon, and S. A. Tretyakov, "Perfect reconfigurable intelligent surfaces with sensing functionality," in *2025 50th International Conference on Infrared, Millimeter, and Terahertz Waves (IRMMW-THz)*, Helsinki, Finland, 2025.

[131] Vuyyuru, S. K. R., R. Valkonen, S. A. Tretyakov, and D.-H. Kwon, "Efficient synthesis of large finite patch arrays for scanning wide-angle anomalous reflectors," *IEEE Open Journal of Antennas and Propagation*, Vol. 6, No. 1, 75–87, 2025.

[132] Bilotti, F., M. Barbuto, Z. Hamzavi-Zarghani, M. Karamirad, M. Longhi, A. Monti, D. Ramaccia, L. Stefanini, A. Toscano, and S. Vellucci, "Reconfigurable intelligent surfaces as the key-enabling technology for smart electromagnetic environments," *Advances in Physics: X*, Vol. 9, No. 1, 2299543, 2024.

[133] Kamenetskii, E., A. Sadreev, and A. Miroshnichenko, *Fano Resonances in Optics and Microwaves*, Springer, 2018.

[134] Silveirinha, M. G., "Broadband negative refraction with a crossed wire mesh," *Physical Review B*, Vol. 79, No. 15, 153109, 2009.

[135] Silveirinha, M. G., "Additional boundary conditions for non-connected wire media," *New Journal of Physics*, Vol. 11, No. 11, 113016, 2009.

[136] Costa, J. T. and M. G. Silveirinha, "Macroscopic electromagnetic response of arbitrarily shaped spatially dispersive bodies formed by metallic wires," *Physical Review B*, Vol. 86, No. 7, 075129, 2012.

[137] Forati, E. and G. W. Hanson, "Scattering from isotropic connected wire medium metamaterials: Three-, two-, and one-dimensional cases," *IEEE Transactions on Antennas and Propagation*, Vol. 61, No. 7, 3564–3574, 2013.

[138] Shin, J., J.-T. Shen, and S. Fan, "Transmission through a scalar wave three-dimensional electromagnetic metamaterial and the implication for polarization control," *Journal of Nanoscience and Nanotechnology*, Vol. 10, No. 3, 1737–1740, 2010.

[139] Schumacher, C., B. Abdennadher, U. Steiner, and M. Saba, "Termination-driven control over bound states in the continuum Q-factors and frequencies in plasmonic double net metamaterials," *ACS Photonics*, Vol. 12, No. 9, 5009–5016, 2025.

[140] Silveirinha, M. G., C. A. Fernandes, and J. R. Costa, "Electromagnetic characterization of textured surfaces formed by metallic pins," *IEEE Transactions on Antennas and Propagation*, Vol. 56, No. 2, 405–415, 2008.

[141] Simovski, C. and S. Tretyakov, *An Introduction to Metamaterials and Nanophotonics*, Cambridge University Press, 2020.

[142] He, S., M. Popov, M. Qiu, and C. Simovski, "An explicit method for the analysis of guided waves in a line-defect channel in a photonic crystal," *Microwave and Optical Technology Letters*, Vol. 26, 67–73, 2000.

[143] Belov, P. A., R. Dubrovka, I. Iorsh, I. Yagupov, and Y. S. Kivshar, "Single-mode subwavelength waveguides with wire metamaterials," *Applied Physics Letters*, Vol. 103, No. 16, 161103, 2013.

[144] Belov, P. A. and M. G. Silveirinha, "Resolution of subwavelength transmission devices formed by a wire medium," *Physical Review E*, Vol. 73, No. 5, 056607, 2006.

[145] Yakovlev, A. B., M. G. Silveirinha, C. R. Simovski, I. S. Nefedov, and S. A. Tretyakov, "Characterization of surface-wave and leaky-wave propagation on wire-medium slabs and mushroom structures based on local and nonlocal homogenization models," *IEEE Transactions on Microwave Theory and Techniques*, Vol. 57, No. 11, 2700–2714, 2009.

[146] Azzam, S. I. and A. V. Kildishev, "Photonic bound states in the continuum: From basics to applications," *Advanced Optical Materials*, Vol. 9, No. 1, 2001469, 2021.

[147] Xu, G., H. Xing, Z. Xue, D. Lu, J. Fan, J. Fan, P. P. Shum, and L. Cong, "Recent advances and perspective of photonic bound states in the continuum," *Ultrafast Science*, Vol. 3, 0033, 2023.

[148] Koshelev, K. L., Z. F. Sadrieva, A. A. Shcherbakov, Y. S. Kivshar, and A. A. Bogdanov, "Bound states in the continuum in photonic structures," *Physics Uspekhi*, Vol. 66, 494–517, 2023.

[149] Koreshin, E., S. Gladyshev, I. Matchenya, R. Balafendiev, I. Terekhov, P. Belov, and A. Bogdanov, "Bound states in the continuum in a wire medium," *Physical Review B*, Vol. 112, No. 8, L081302, Aug. 2025.

[150] Balafendiev, R., C. Simovski, A. J. Millar, and P. Belov, "Wire metamaterial filled metallic resonators," *Physical Review B*, Vol. 106, No. 7, 075106, 2022.

[151] Vovchuk, D., M. Khobzei, M. Apostoliuk, V. Tkach, and C. Simovski, "Broadband transfer of binary images via optically long wire media," *Nanophotonics*, Vol. 12, No. 14, 2797–2807, 2023.

[152] Khobzei, M., V. Tkach, S. Haliuk, A. Samila, V. Bobrovs, P. Ginzburg, C. Simovski, and D. Vovchuk, "Deformable wire media resonators," in *2024 Eighteenth International Congress on Artificial Materials for Novel Wave Phenomena (Metamaterials)*, 1–4, Chania, Greece, 2024.

[153] Adams, C. B., N. Aggarwal, A. Agrawal, R. Balafendiev, C. Bartram, M. Baryakhtar, H. Bekker, P. Belov, K. K. Berggren, A. Berlin, *et al.*, "Axion dark matter," *arXiv preprint arXiv:2203.14923*, 2022.

[154] Millar, A. J., S. M. Anlage, R. Balafendiev, P. Belov, K. Van Bibber, J. Conrad, M. Demarteau, A. Droster, K. Dunne, *et al.*, "Searching for dark matter with plasma haloscopes," *Physical Review D*, Vol. 107, No. 5, 055013, 2023.

[155] Enriquez, J. A., R. Balafendiev, A. J. Millar, C. Simovski, and P. Belov, "Uniform field in microwave cavities through the use of effective magnetic walls," *Physical Review Applied*, Vol. 23, No. 5, 054053, 2025.

[156] Al-Rubaiee, M., A. Alchalaby, and H. Al-Janabi, "Subwavelength wire array metamaterial microwave cavities," *Nanophotonics Australasia 2017*, Vol. 10456, 104565J, 2018.

[157] Belov, P. A., Y. Hao, and S. Sudhakaran, "Subwavelength microwave imaging using an array of parallel conducting wires as a lens," *Physical Review B*, Vol. 73, No. 3, 033108, 2006.

[158] Silveirinha, M. G., P. A. Belov, and C. R. Simovski, "Subwavelength imaging at infrared frequencies using an array of metallic nanorods," *Physical Review B*, Vol. 75, No. 3, 035108, 2007.

[159] Silveirinha, M. G., C. R. Medeiros, C. A. Fernandes, and J. R. Costa, "Resolving subwavelength objects with a crossed wire mesh superlens operated in backscattering mode," *New Journal of Physics*, Vol. 13, No. 5, 053004, 2011.

[160] Habib, M. S., A. Tuniz, K. J. Kaltenecker, Q. Chateiller, I. Perrin, S. Atakaramians, S. C. Fleming, A. Argyros, and B. T. Kuhlmey, "Removing image artefacts in wire array metamaterials," *Optics Express*, Vol. 24, No. 16, 17 989–18 002, 2016.

[161] Belov, P. A., C. R. Simovski, and P. Ikonen, "Canalization of subwavelength images by electromagnetic crystals," *Physical Review B*, Vol. 71, No. 19, 193105, 2005.

[162] Belov, P. A., Y. Zhao, S. Tse, P. Ikonen, M. G. Silveirinha, C. R. Simovski, S. Tretyakov, Y. Hao, and C. Parini, "Transmission of images with subwavelength resolution to distances of several wavelengths in the microwave range," *Physical Review B*, Vol. 77, No. 19, 193108, 2008.

[163] Zhao, Y., G. Palikaras, P. A. Belov, R. F. Dubrovka, C. R. Simovski, Y. Hao, and C. G. Parini, "Magnification of subwavelength field distributions using a tapered array of metallic wires with planar interfaces and an embedded dielectric phase compensator," *New Journal of Physics*, Vol. 12, No. 10, 103045, 2010.

[164] Slobozhanyuk, A. P., I. V. Melchakova, C. R. Simovski, and P. A. Belov, "Experimental verification of enhancement of evanescent waves inside a wire medium," *Applied Physics Letters*, Vol. 103, No. 5, 051118, 2013.

[165] Kosulnikov, S., D. Filonov, S. Glybovski, P. Belov, S. Tretyakov, and C. Simovski, "Wire-medium hyperlens for enhancing radiation from subwavelength dipole sources," *IEEE Transactions on Antennas and Propagation*, Vol. 63, No. 11, 4848–4856, 2015.

[166] Citroni, R., F. Di Paolo, and A. Di Carlo, "Replacing noble metals with alternative metals in MID-IR frequency: A theoretical approach," *AIP Conference Proceedings*, Vol. 1990, No. 1, 020004, 2018.

[167] Morgado, T. A. and M. G. Silveirinha, "Focusing of electromagnetic radiation by a flat slab of a crossed wire mesh metamaterial," *Metamaterials*, Vol. 4, No. 2–3, 112–118, 2010.

[168] Matchenya, I., G. Karsakov, and E. Koreshin, "Wide-angle broadband metamaterial lens based on double wire medium," in *2023 Seventeenth International Congress on Artificial Materials for Novel Wave Phenomena (Metamaterials)*, X–168–X–170, Chania, Greece, 2023.

[169] Pelton, M., "Modified spontaneous emission in nanophotonic structures," *Nature Photonics*, Vol. 9, No. 7, 427–435, 2015.

[170] Simovski, C., "Circuit model of plasmon-enhanced fluorescence," *Photonics*, Vol. 2, No. 2, 568–593, 2015.

[171] Krasnok, A. E., A. P. Slobozhanyuk, C. R. Simovski, S. A. Tretyakov, A. N. Poddubny, A. E. Miroshnichenko, Y. S. Kivshar, and P. A. Belov, "An antenna model for the Purcell effect," *Scientific Reports*, Vol. 5, No. 1, 12956, 2015.

[172] Poddubny, A. N., P. A. Belov, and Y. S. Kivshar, "Purcell effect in wire metamaterials," *Physical Review B*, Vol. 87, No. 3, 035136, 2013.

[173] Mirmoosa, M. S., S. Y. Kosulnikov, and C. R. Simovski, "Magnetic hyperbolic metamaterial of high-index nanowires," *Physical Review B*, Vol. 94, No. 7, 075138, 2016.

[174] Mirmoosa, M. S., S. Y. Kosulnikov, and C. R. Simovski, "Double resonant wideband Purcell effect in wire metamaterials," *Journal of Optics*, Vol. 18, No. 9, 095101, 2016.

[175] Burghignoli, P., G. Lovat, F. Capolino, D. R. Jackson, and D. R. Wilton, "Directive leaky-wave radiation from a dipole source in a wire-medium slab," *IEEE Transactions on Antennas and Propagation*, Vol. 56, No. 5, 1329–1339, 2008.

[176] Li, Y. and M. G. Silveirinha, "Radiation from a Hertzian dipole embedded in a wire-medium slab," *IEEE Antennas and Wireless Propagation Letters*, Vol. 12, 401–404, 2013.

[177] Wilczek, F., "Two applications of axion electrodynamics," *Physical Review Letters*, Vol. 58, No. 18, 1799, 1987.

[178] Dine, M. and W. Fischler, "The not-so-harmless axion," *Physics Letters B*, Vol. 120, No. 1–3, 137–141, 1983.

[179] Preskill, J., M. B. Wise, and F. Wilczek, "Cosmology of the invisible axion," *Physics Letters B*, Vol. 120, No. 1–3, 127–132, 1983.

[180] Sushkov, A. O., "Quantum science and the search for axion dark matter," *PRX Quantum*, Vol. 4, No. 2, 020101, 2023.

[181] Sikivie, P., "Experimental tests of the "invisible" axion," *Physical Review Letters*, Vol. 51, No. 16, 1415, 1983.

[182] Feng, J. L., "Dark matter candidates from particle physics and methods of detection," *Annual Review of Astronomy and Astrophysics*, Vol. 48, 495–545, 2010.

[183] Buschmann, M., J. W. Foster, A. Hook, A. Peterson, D. E. Willcox, W. Zhang, and B. R. Safdi, "Dark matter from axion strings with adaptive mesh refinement," *Nature Communications*, Vol. 13, No. 1, 1049, 2022.

[184] Caldwell, A., G. Dvali, B. Majorovits, A. Millar, G. Raffelt, J. Redondo, O. Reimann, F. Simon, and F. Steffen, "Dielectric haloscopes: A new way to detect axion dark matter," *Physical Review Letters*, Vol. 118, 091801, 2017.

[185] Lawson, M., A. J. Millar, M. Pancaldi, E. Vitagliano, and F. Wilczek, "Tunable axion plasma haloscopes," *Physical Review Letters*, Vol. 123, No. 14, 141802, 2019.

[186] Balafendiev, R., G. Kaur, J. A. Enriquez, G. Singh, A. J. Millar, J. E. Gudmundsson, and P. Belov, "Tunable epsilon near zero metamaterial with rotating obround-shaped meta-atoms," *arXiv preprint arXiv:2506.04428*, 2025.

[187] Sakhno, D., J. A. Enriquez, and P. A. Belov, "Volume-preserving deformation of honeycomb wire media enables broad plasma frequency tunability," *Physical Review Applied*, Vol. 24, L051001, Nov. 2025.

[188] Simovski, C., S. Maslovski, I. Nefedov, and S. Tretyakov, "Optimization of radiative heat transfer in hyperbolic metamaterials for thermophotovoltaic applications," *Optics Express*, Vol. 21, No. 12, 14 988–15 013, 2013.

[189] Shvets, G., S. Trendafilov, J. B. Pendry, and A. Sarychev, "Guiding, focusing, and sensing on the subwavelength scale using metallic wire arrays," *Physical Review Letters*, Vol. 99, No. 5, 053903, 2007.

[190] Nieminen, T., P. Lähteenmäki, Z. Tan, D. Cox, and P. J. Hakonen, "Low-noise correlation measurements based on software-defined-radio receivers and cooled microwave amplifiers," *Review of Scientific Instruments*, Vol. 87, No. 11, 114706, 2016.